Electronic Supplementary Information for:

Exploring the Triplet State Properties of Thio-Benzothioxanthene Imides with Applications in TTA-Upconversion and Photopolymerization

Xiaoping Chen, Hui Liang*, Xitong He, Weiqiang Li, Zhiyao Nian, Zafar Mahmood, Yanping Huo, Shaomin Ji*

School of Chemical Engineering and Light Industry, Guangdong University of Technology, Guangzhou, 510006, PR China

Corresponding author. E-mail address: *smji@gdut.edu.cn*

Index

1. Methods

General Information

All of the chemicals used in the synthesis were of analytical grade. The solvents were dried prior to their use in the synthesis. ^{1}H NMR and ^{13}C NMR were carried out using NMR AVANCE III HD 400 spectrometer. The HRMS spectra of the compounds were investigated by means of a thermo scientifc Q executive spectrometer. UV-VIS 2700 spectrophotometer (Shimadzu Ltd, Japan) was used to measure UV-VIS absorption spectra of samples. Steady state fluorescence emission spectra were obtained using a homemade spectrometer (IDR-MICRO-532-2/QEPRO-ABS/NIRQUEST512, Ocean optics). Time resolved fluorescence spectra were recorded using the FLS980 spectrophotometer (Edinburgh Instruments Ltd, UK, TCSPC mode), 374 nm picosecond pulsed laser, the repetition rates of the EPL picosecond laser for different lifetime ranges were 10 MHz for 100 ns detection window.

Nanosecond Transient Absorption Spectroscopy

Nanosecond transient absorption spectra were measured on an LP980 laser flash photolysis spectrometer (Edinburgh Instruments, UK). The signal was digitized using a Tektronix MDO 3022 oscilloscope, and all samples were degassed with argon for approximately 15 minutes prior to measurement. L900 software was used to process the kinetic decay traces and fitting data.

Determination of Singlet Oxygen Quantum Yield

The singlet oxygen quantum yield (Φ_Δ) of the dyads was determined using 1,3-diphenylisobenzofuran (DPBF) as a singlet oxygen scavenger. By following the change in absorbance (λ_{max} = 414 nm) of DPBF upon photoexcitation of the mixture, the singlet oxygen quantum yield was determined using the equation. BDP-2I was used as a standard for **BTXI-LS**, **BTXI-RS** and **BTXI-DS** (BDP-2I in ACN, Φ_{std} = 87%).[1] Ru(bpy)$_3$(PF$_6$)$_2$ was used as a standard for **BTXI** ((Ru(bpy)$_3$(PF$_6$)$_2$ in DCM, Φ_{std} = 57%).[2] Φ is the singlet oxygen quantum yield. A is the absorbance at the excitation wavelength (A = 0.2~0.3). K is the slope. η represents the refractive index of the solvent.

$$\Phi_{sam} = \Phi_{std} \left(\frac{1 - 10^{-A^{std}}}{1 - 10^{-A^{sam}}} \right) \left(\frac{k_{sam}}{k_{std}} \right) \left(\frac{\eta_{sam}}{\eta_{std}} \right)^2$$

Triplet-Triplet Annihilation (TTA)-Upconversion

TTA upconversion is performed by adjusting the concentration of photosensitizer ($c \approx 1 \times 10^{-5}$ M) and acceptor ($c \approx 1 \times 10^{-4}$ M). The samples were bubbled with argon for 15 minutes prior to measurements. Upconversion was performed with 561/635 nm CW laser (Changchun Radium Optoelectronics Technology Co., Ltd.) as excitation source, the power intensity was detected by power meters (S130C, Thorlabs), upconversion emission spectra was record by spectra detector (IDR-MICRO-532-2/QEPRO-ABS/NIRQUEST512, Ocean optics). Upconversion quantum yield is calculated using following equations (The maximum Φ_{UC} value is 100%). Φ_{std} represent the luminescence quantum yield of the reference. BDP-2I was used as a standard for **BTXI-LS** and **BTXI-RS** (BDP-2I in ACN, Φ_{std} = 2.7%)[1], and upconversion was performed with 561 nm CW laser. Methylene blue was used as a standard for **BTXI-DS** (methylene blue in MeOH, Φ_{std} = 3%)[2] and upconversion was performed with 635 nm CW laser. A_{std} and A_{UC} represent the absorbance at 561/635 nm CW laser of the reference and upconversion systems, respectively. I_{uc} and I_{std} represent the integrated areas of the peaks occurring in the upconversion system and the reference, respectively. η represents the refractive index of the solvent. The upconversion quantum yield is normalized upconversion intensity, a factor of 2 was used in the calculation.

$$\Phi_{UC} = 2 \times \Phi_{std} \times \left(\frac{1 - 10^{-A^{std}}}{1 - 10^{-A^{UC}}}\right) \times \left(\frac{I_{UC}}{I_{std}}\right) \times \left(\frac{\eta_{UC}}{\eta_{std}}\right)^2$$

Density Functional Theory Calculations

To optimize the ground state geometry and to calculate the excited state energy levels of the samples, the PBE0 functional and the 6-31G (d,p) basis with density functional theory (DFT) and its time dependent extension (TDDFT) levels were used, respectively. The triplet excited state spin density surfaces of the samples were calculated on the basis of the DFT//PBE0/6-31G (d,p)-optimized ground state geometries. The Gaussian 16 program package was used for the calculation.[3]

Photopolymerization

Photoinitiators (0.02 mmol%), diphenyliodonium salt (0.05 mmol%), were mixed with 10 mmol of olefin monomer. All samples were degassed with argon for approximately 15 minutes prior to irradiation. After the deoxygenation was completed，the **BTXI-RS** samples were irradiated by 532 nm optical fiber, while the **BTXI-DS** samples were irradiated by 630 nm LED light for 5 minutes (100 mW cm^{-2}).

2. Synthesis of compounds
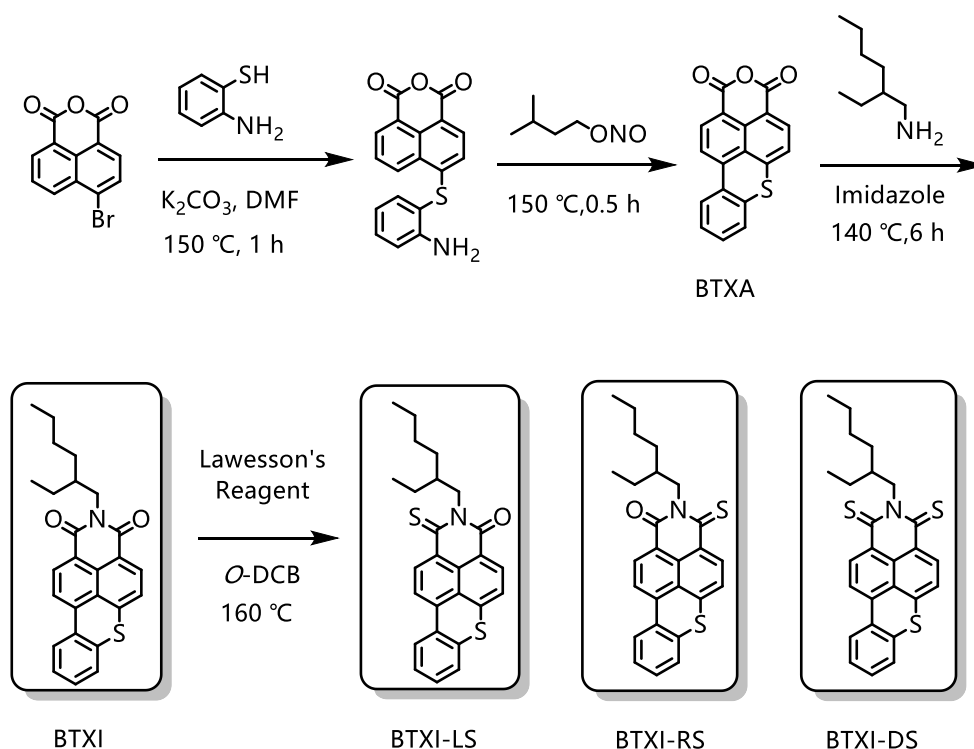
Scheme S1: The synthetic route of the compounds.

BTXA were synthesized according to literature method.[4,5]

Compound **BTXI**. The mixture of BTXA (2.5 g, 8.2 mmol), imidazole (16.1 g, 236.7 mmol), and 2-ethylhexylamine (4.5 mL, 27.9 mmol) was stirred for 6 hours under N$_2$ atmosphere at 140 ℃. After cooling to room temperature, the product was extracted with dichloromethane and water, and dried with anhydrous sodium sulfate. The solvent was then evaporated under reduced pressure. The crude product was purified by column chromatography (silica gel, dichloromethane: petroleum ether = 1:1) to give a yellow product (2.2 g) in a yield of 64%. ^{1}H NMR (400 MHz, CDCl$_3$) δ 8.46 (d, J = 8.0 Hz, 1H), 8.29 (d, J = 8.0 Hz, 1H), 8.03 (dd, J = 20.0, 8.0 Hz, 2H), 7.43-7.28 (m, 4H), 4.16 -3.98 (m, 2H), 1.93 (s, 1H), 1.45-1.29 (m, 8H), 0.97-0.84 (m, 6H). ^{13}C NMR (100 MHz, CDCl$_3$) δ 164.13, 163.68, 140.17, 136.32, 132.38, 131.53, 130.65, 130.20, 129.84, 127.80, 127.48, 126.32, 125.92, 125.25, 121.16, 120.23, 119.02, 118.02, 44.18, 37.85, 30.80, 28.75, 24.10, 23.12, 14.13, 10.68. HRMS m/z calculated for C$_{26}$H$_{25}$NO$_2$S [(M+H)$^+$]: 416.16788, observed: 416.16791.

Compound **BTXI-LS** and **BTXI-RS**. BTXI (200 mg, 0.48 mmol), Lawesson's Reagent (400 mg, 0.96 mmol) were dissolved in 1,2-dichlorobenzene (5 mL) under an N$_2$

atmosphere, and the reaction mixture was heated to 160 °C and refluxed for 2 hours under stirring. After cooling to room temperature, add water to the product, and then evaporated under reduced pressure to remove 1,2-dichlorobenzene. The solvent was then extracted with dichloromethane and water, and dried with anhydrous sodium sulfate. And the solvent then was evaporated under reduced pressure. The crude product was purified by column chromatography (silica gel, ethyl acetate: petroleum ether = 1:20) to give **BTXI-LS** and **BTXI-RS** in the following yields.

BTXI-LS (21 mg, 10 %). ^{1}H NMR (400 MHz, CDCl$_3$) δ 9.07 (d, J = 8.0 Hz, 1H), 8.41 (d, J = 8.0 Hz, 1H), 8.26-8.03 (m, 2H), 7.54-7.33 (m, 4H), 4.83-4.61 (m, 2H), 2.23 (s, 1H), 1.47-1.35 (m, 8H), 0.96-0.85 (m, 6H). ^{13}C NMR (100 MHz, CDCl$_3$) δ 193.00, 162.05, 140.97, 138.45, 136.06, 131.81, 131.72, 130.03, 128.59, 128.01, 127.75, 126.78, 126.34, 126.15, 125.34, 120.88, 119.66, 118.44, 50.70, 36.69, 30.74, 28.67, 24.09, 23.15, 14.13, 10.82. HRMS m/z calculated for C$_{26}$H$_{25}$NOS$_2$ [(M+H)[+]]: 432.14503, observed: 432.14545.

BTXI-RS (13 mg, 6%). ^{1}H NMR (400 MHz, CDCl$_3$) δ 8.88 (s, 1H), 8.56 (s, 1H), 8.14 (d, J = 16.0 Hz, 2H), 7.39 (s, 4H), 4.72 (t, J = 8.0 Hz, 2H), 2.22 (s, 1H), 1.49-1.34 (m, 8H), 0.95-0.86 (m, 6H). ^{13}C NMR (100 MHz, CDCl$_3$) δ 193.55, 161.52, 140.57, 136.55, 133.57, 133.55, 131.67, 130.03, 128.47, 127.75, 126.44, 126.20, 124.99, 124.38, 124.26, 123.48, 121.53, 120.91, 119.61, 50.65, 36.75, 30.73, 28.67, 24.07, 23.16, 14.14, 10.81. HRMS m/z calculated for C$_{26}$H$_{25}$NOS$_2$ [(M+H)[+]]: 432.14503, observed: 432.14520.

Compound **BTXI-DS**. BTXI (200 mg, 0.48 mmol), Lawesson's Reagent (600 mg, 1.44 mmol) were dissolved in 1,2-dichlorobenzene (5 mL) under an N$_2$ atmosphere, and the reaction mixture was heated to 160 °C and refluxed for 3 hours under stirring. After cooling to room temperature, add water to the product, and then evaporated under reduced pressure to remove 1,2-dichlorobenzene. The solvent was then extracted with dichloromethane and water, and dried with anhydrous sodium sulfate. And the solvent then was evaporated under reduced pressure. The crude product was purified by column chromatography (silica gel, petroleum ether) to give a blue product (20 mg) in a yield of 9%. ^{1}H NMR (400 MHz, CDCl$_3$) δ 8.99 (d, J = 12.0 Hz, 1H), 8.82 (d, J = 8.0 Hz, 1H), 8.24-8.15 (m, 1H), 8.09 (d, J = 12.0 Hz, 1H), 7.53-7.35 (m, 4H), 5.65-5.43 (m, 2H), 2.48-2.33 (m, 1H), 1.51-1.21 (m, 8H), 0.97-0.78 (m, 6H). ^{13}C NMR (100 MHz, CDCl$_3$) δ 141.08, 135.95, 131.90, 130.16, 128.73, 127.98, 127.87, 126.39, 126.30, 125.31, 124.93, 121.72, 120.39, 57.44, 36.94, 30.63, 28.74, 24.00, 23.16, 14.13, 11.13. HRMS m/z calculated for C$_{26}$H$_{25}$NS$_3$ [(M+H)[+]]: 448.12219, observed: 448.12111.

3. Molecular structure characterization
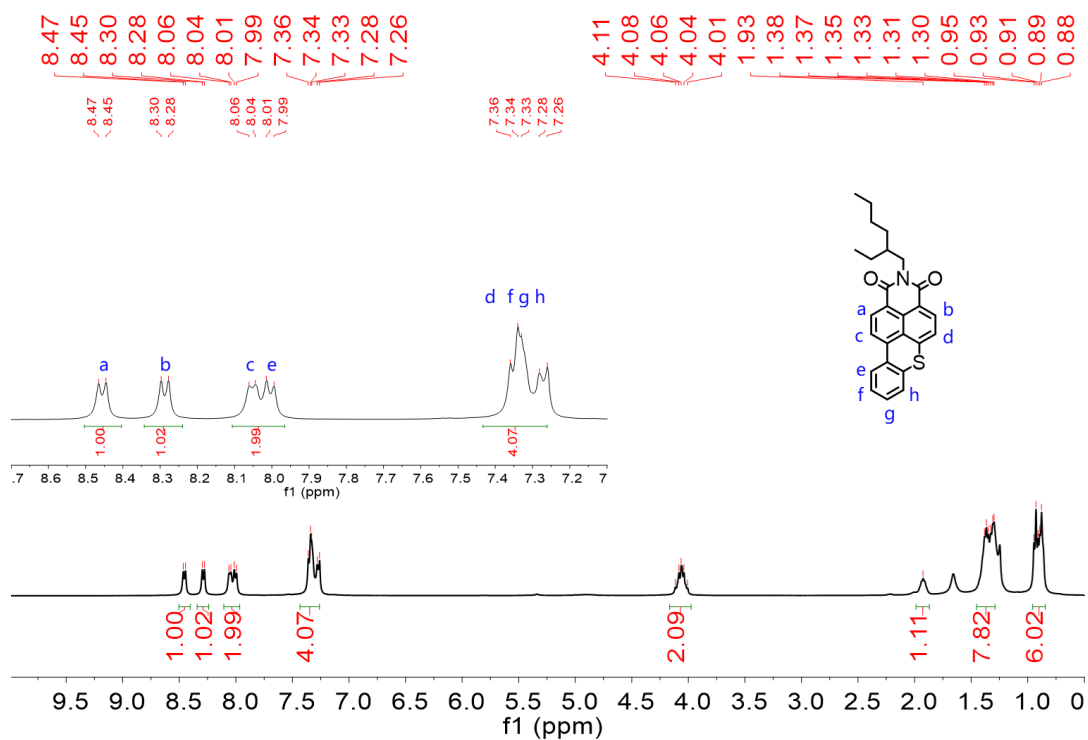
Figure S1. ^{1}H NMR spectra of **BTXI**.
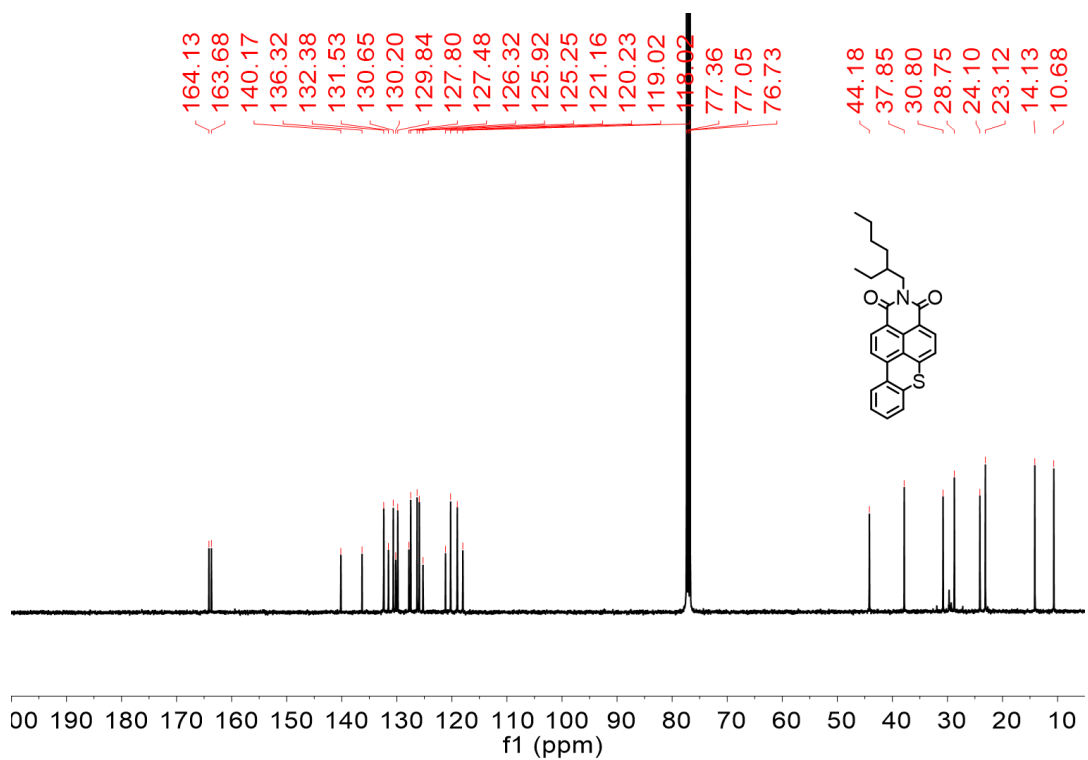
Figure S2. ^{13}C NMR spectra of **BTXI**.
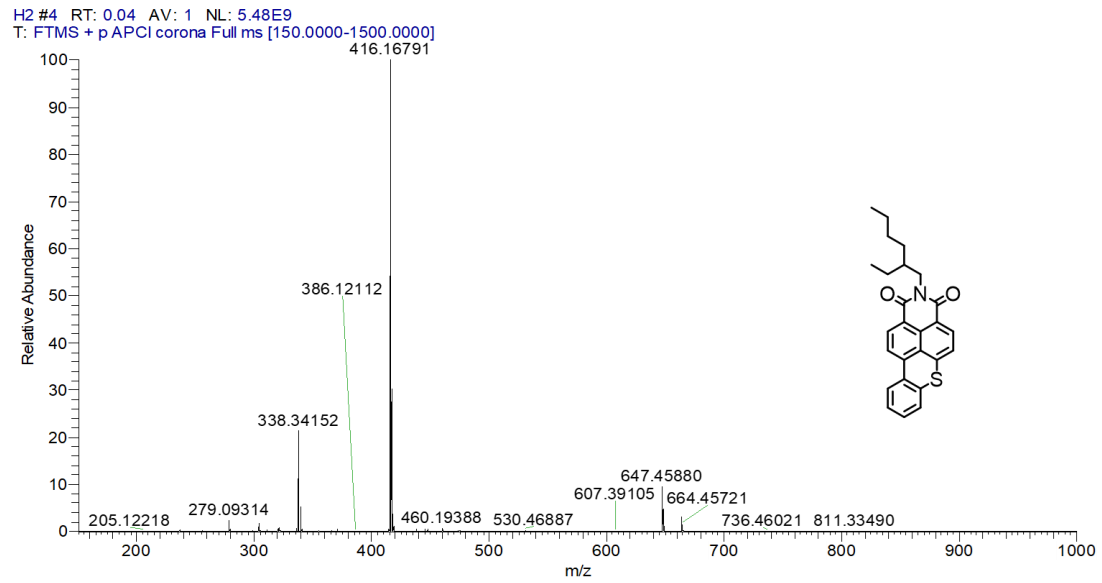
Figure S3. HRMS spectra of **BTXI**.
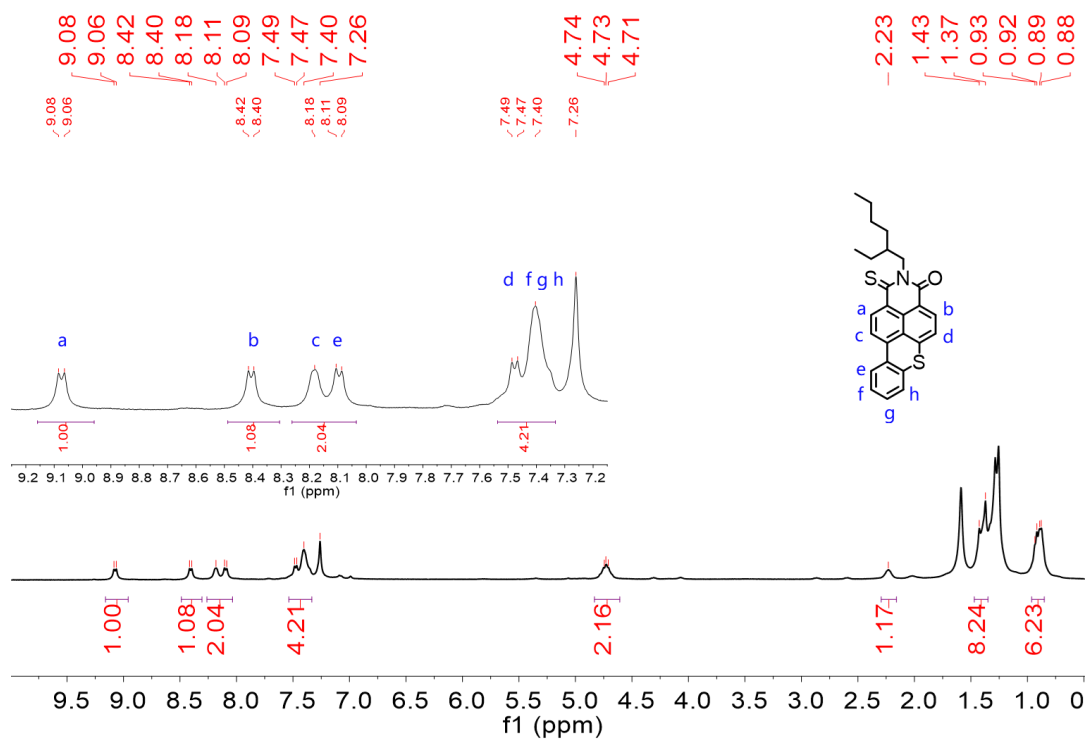
Figure S4. ^{1}H NMR spectra of **BTXI-LS**.
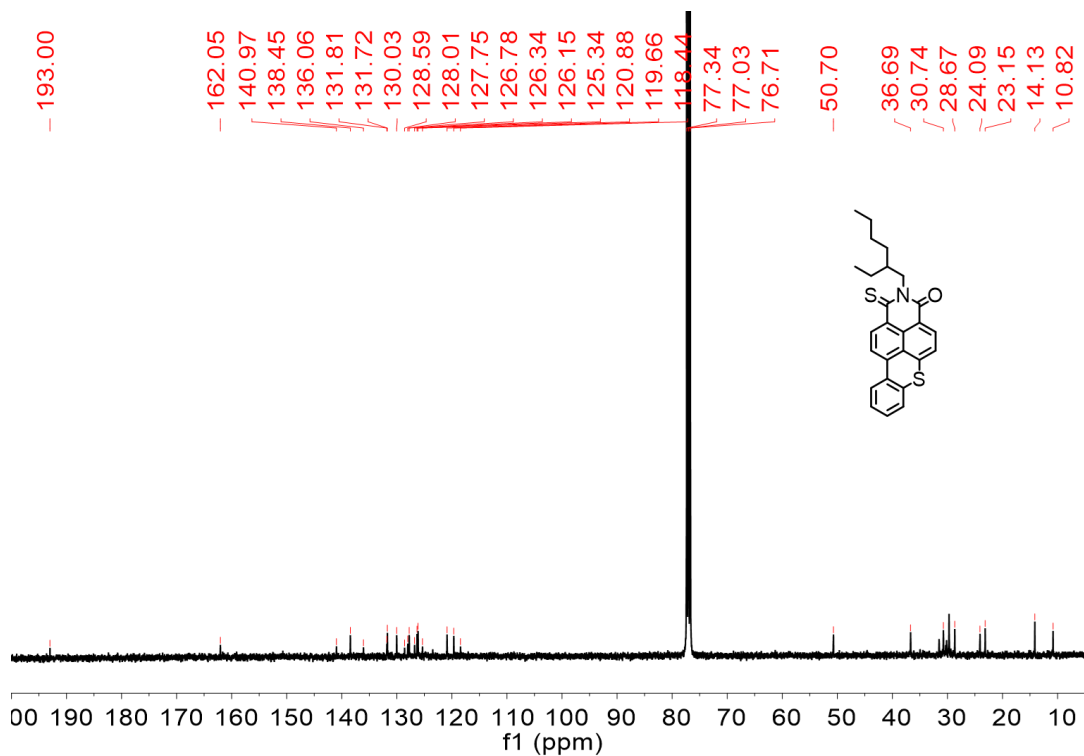
Figure S5. ^{13}C NMR spectra of **BTXI-LS**.
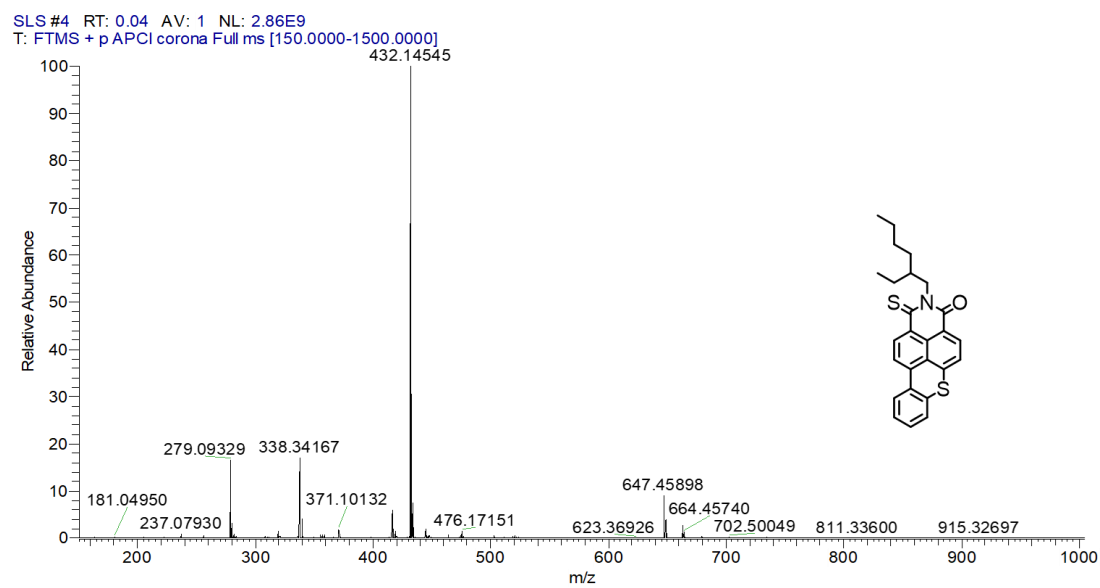
Figure S6. HRMS spectra of **BTXI-LS**.
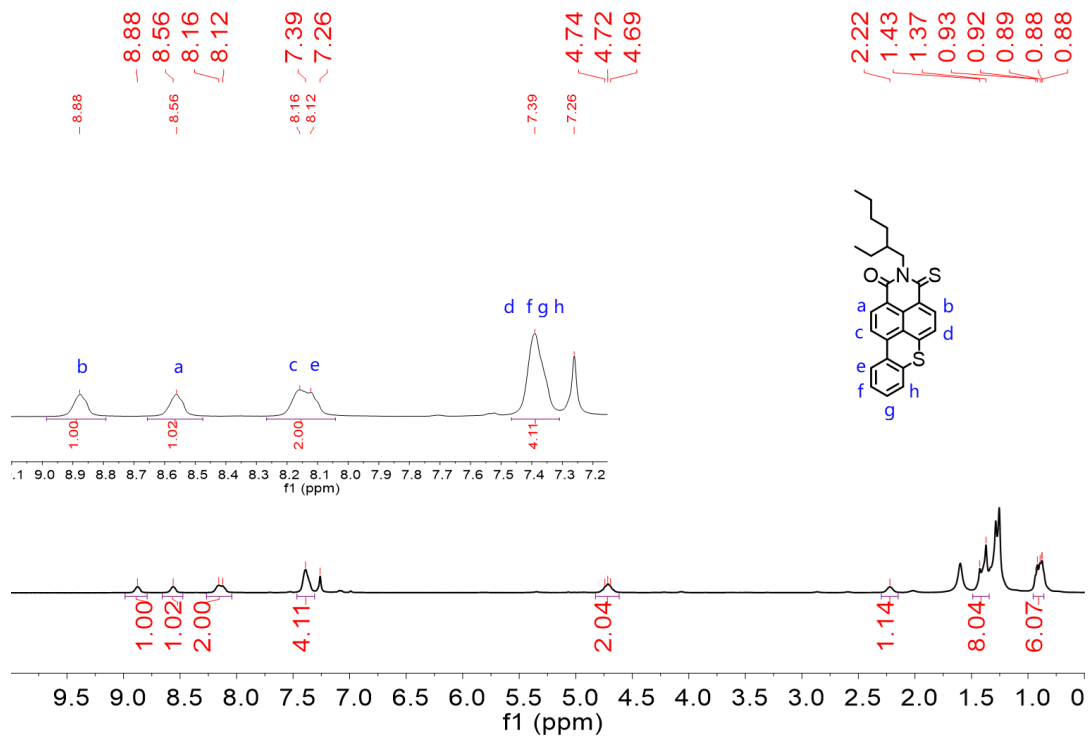
Figure S7. ^{1}H NMR spectra of **BTXI-RS**.
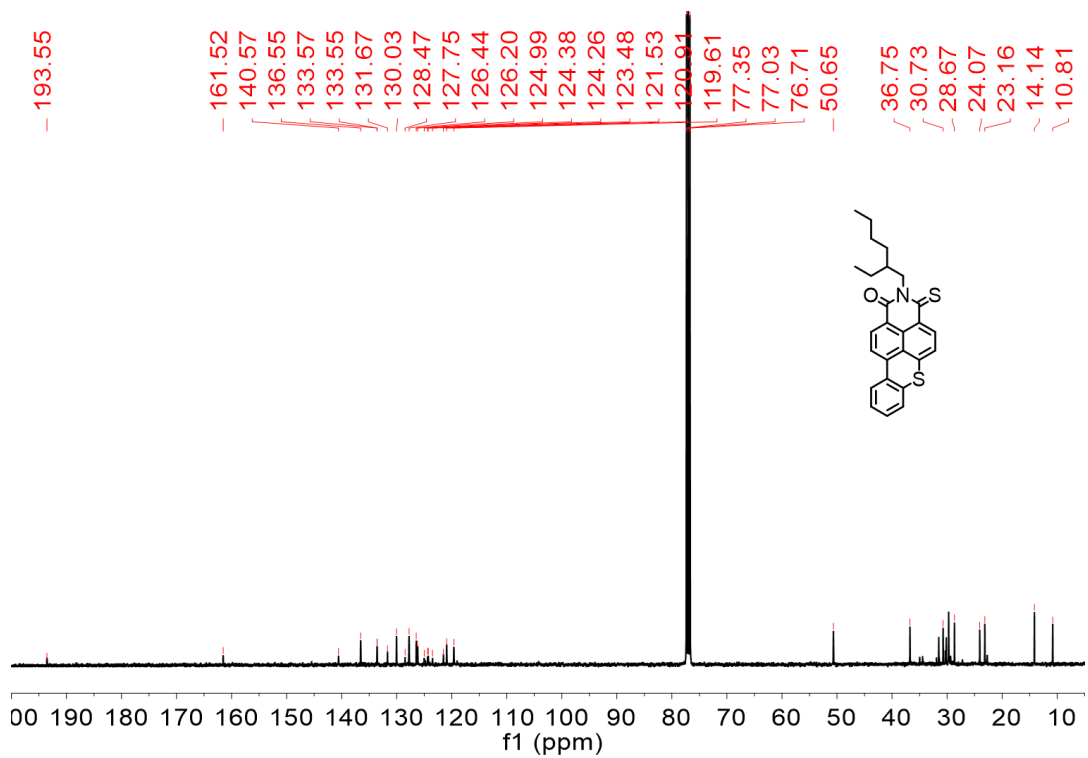
Figure S8. ^{13}C NMR spectra of **BTXI-RS**.
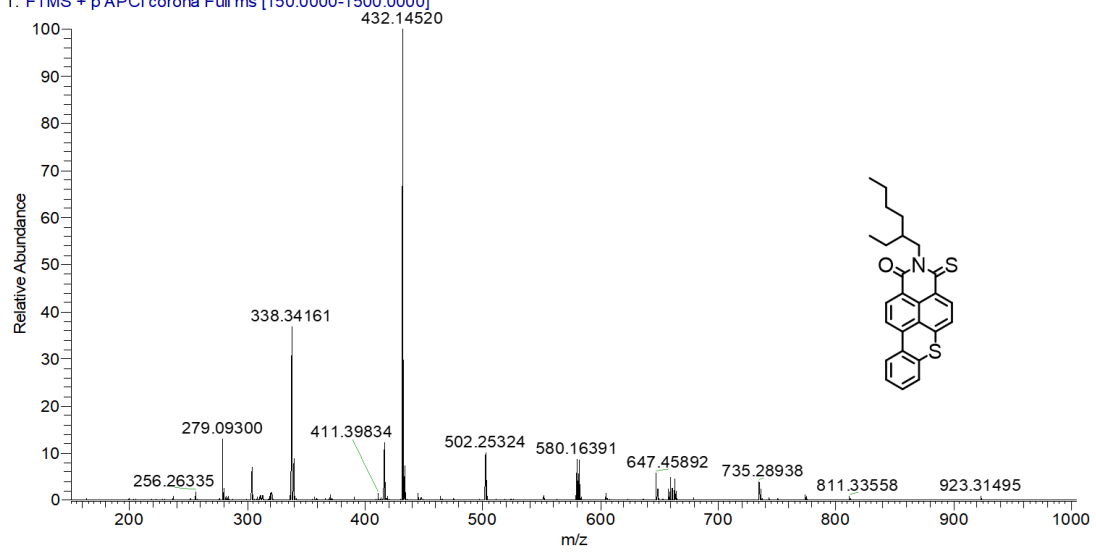
Figure S9. HRMS spectra of **BTXI-RS**.
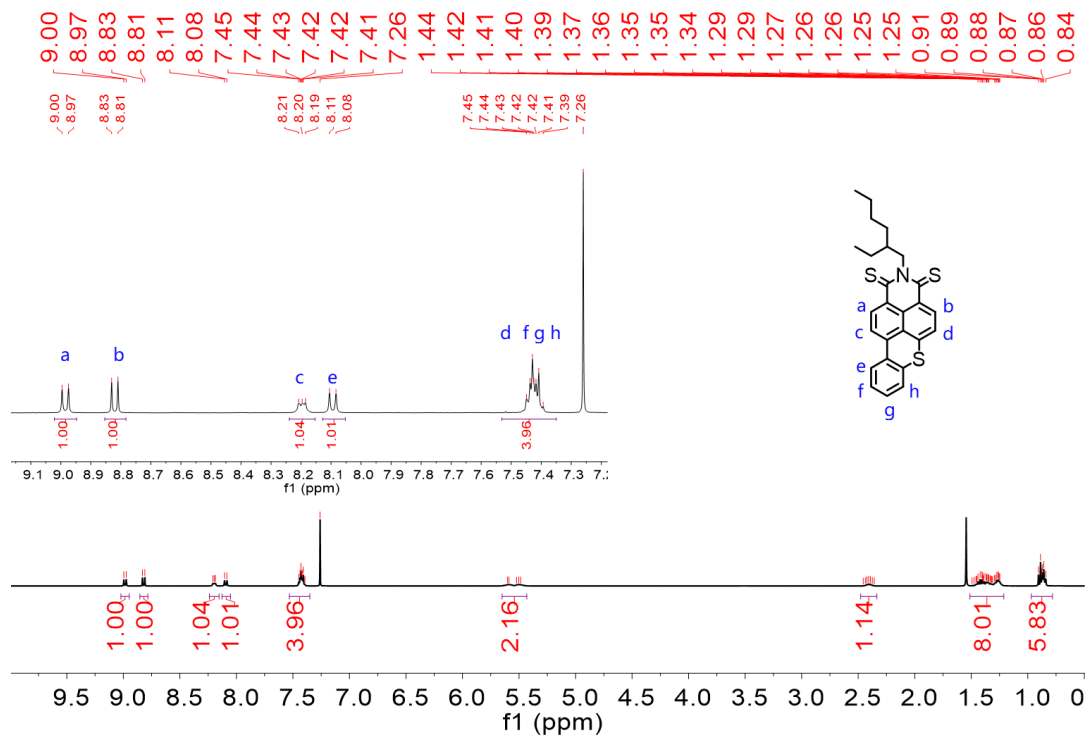
Figure S10. ^{1}H NMR spectra of **BTXI-DS**.
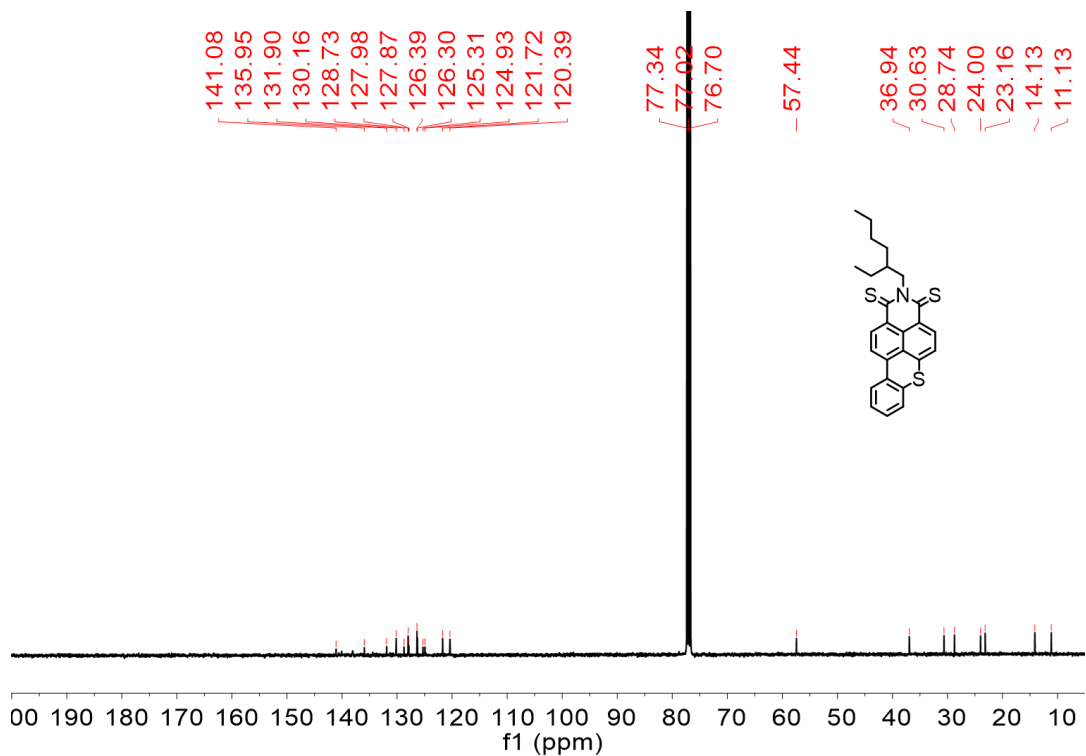
Figure S11. ^{13}C NMR spectra of **BTXI-DS**.
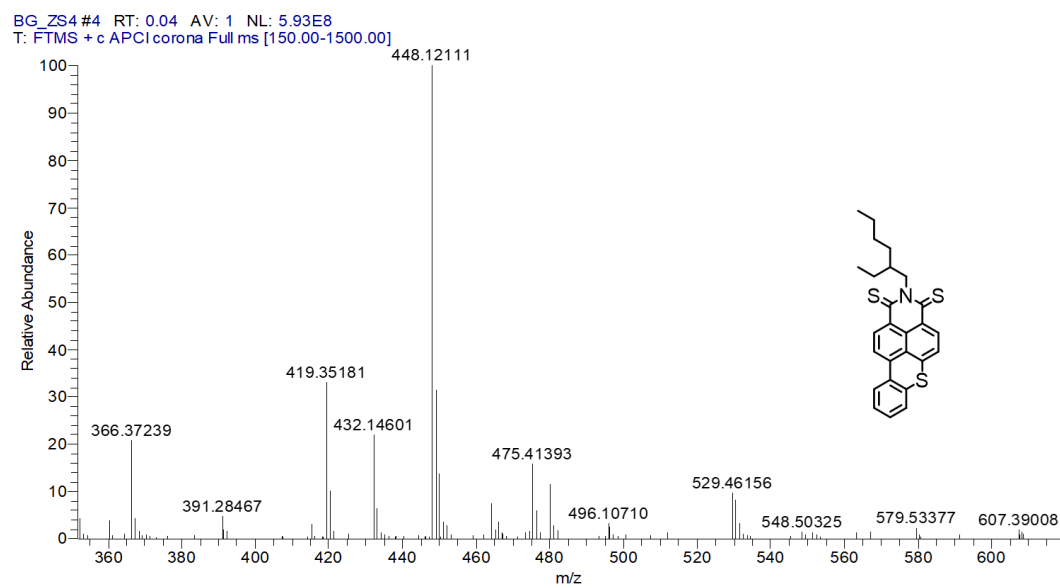
Figure S12. HRMS spectra of **BTXI-DS**.
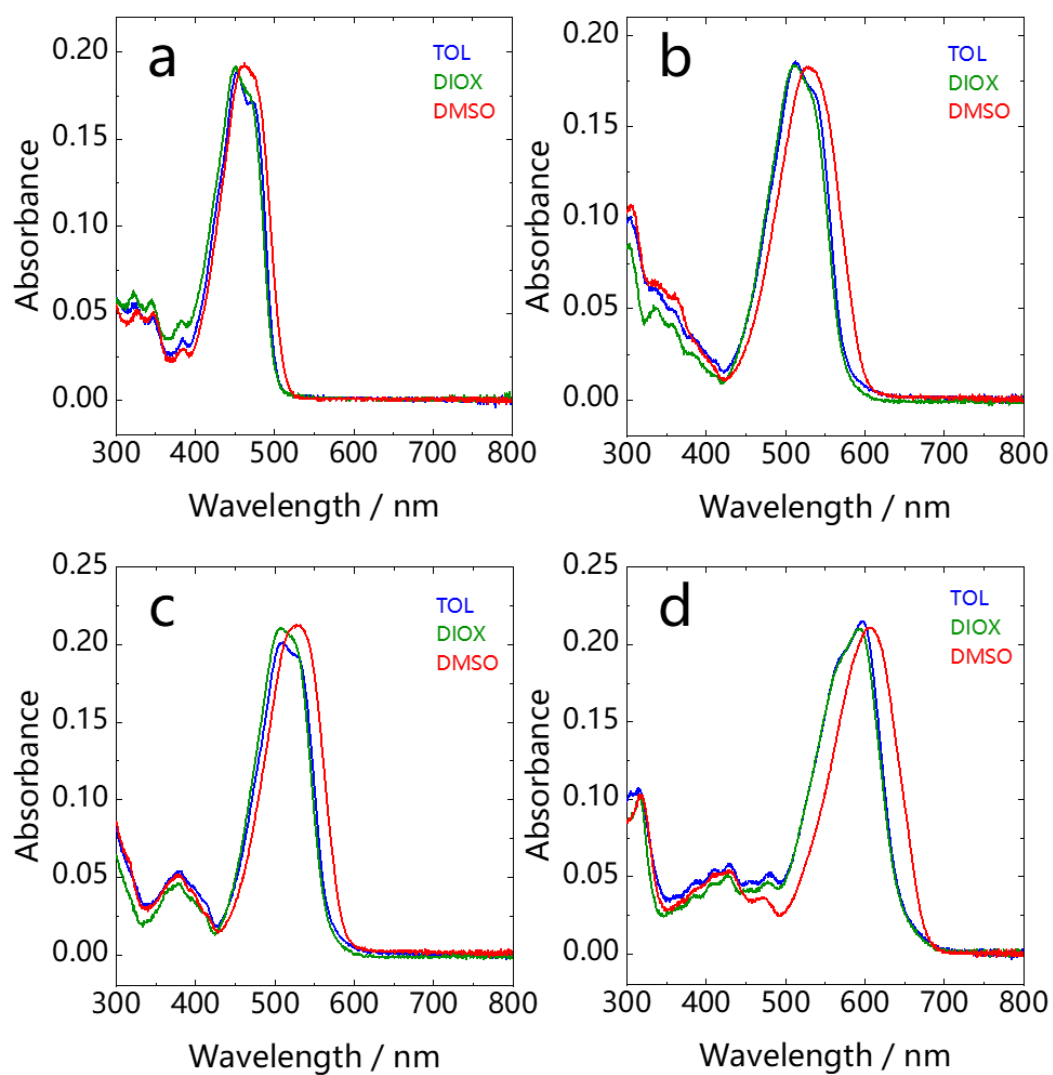
4. UV-Vis absorption spectra

Figure S13. UV-Vis absorption spectra of **BTXI** (a), **BTXI-LS** (b), **BTXI-RS** (c) and **BTXI-DS** (d) in different solvents, $c \approx 1 \times 10^{-5}$ M.

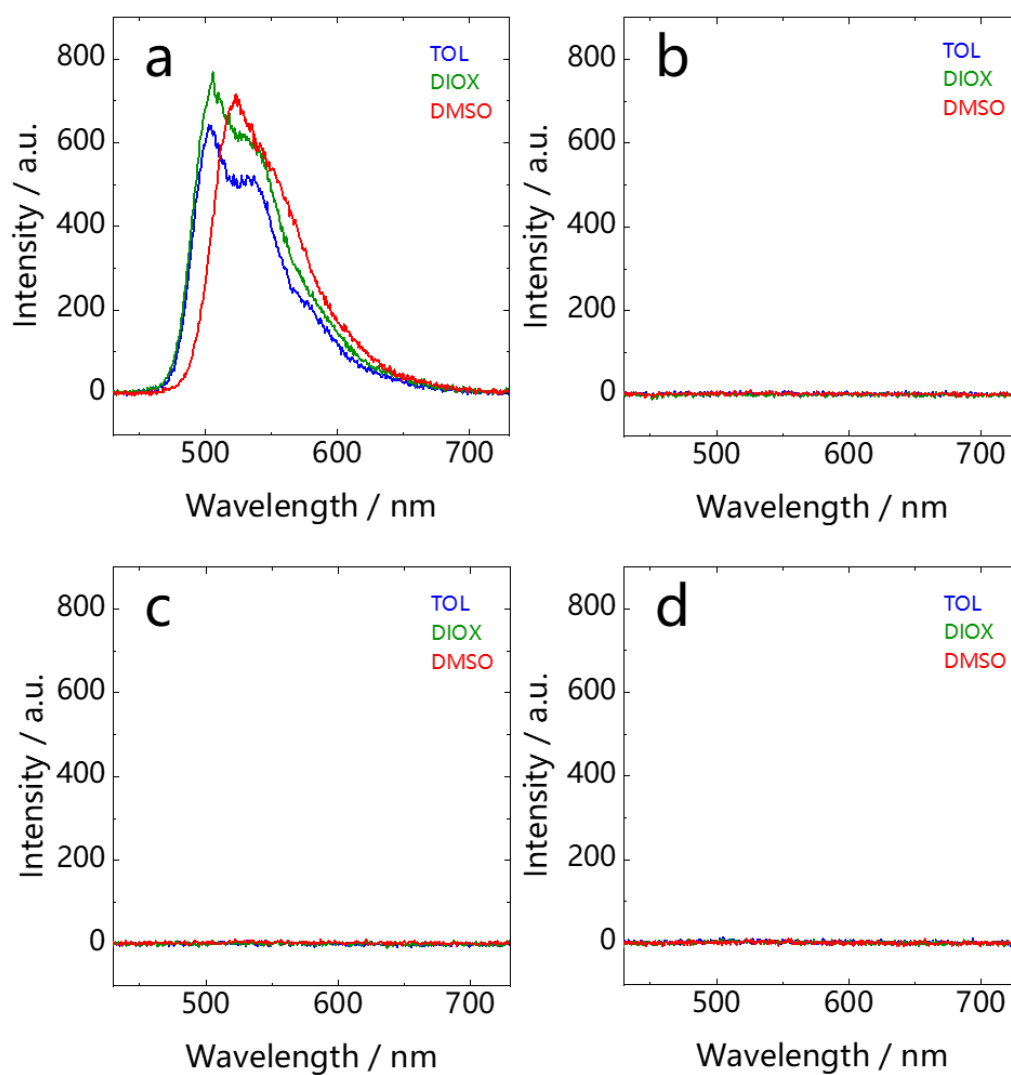## 5. Steady and Transient Fluorescence Emission Spectra

Figure S14. Fluorescence emission spectra of **BTXI** (a), **BTXI-LS** (b), **BTXI-RS** (c) and **BTXI-DS** (d) in different solvents. Condition: $A \approx 0.03$, λ_{ex} = 420 nm.

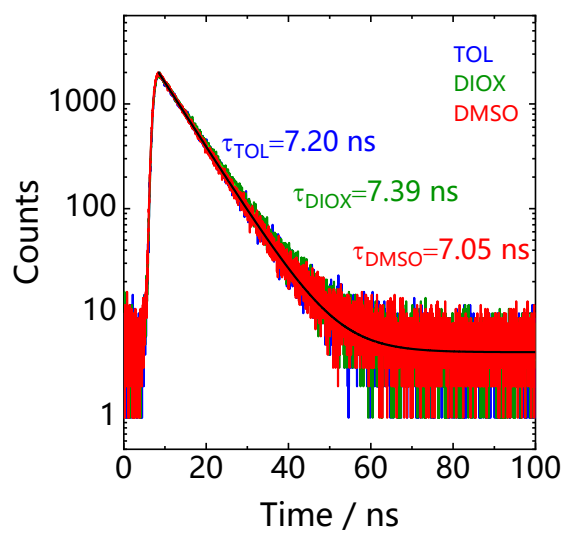**Figure S15.** The decay curves of **BTXI** at the maximum emission wavelength in different solvents, respectively. $c \approx 1 \times 10^{-5}$ M, λ_{ex} = 374 nm.
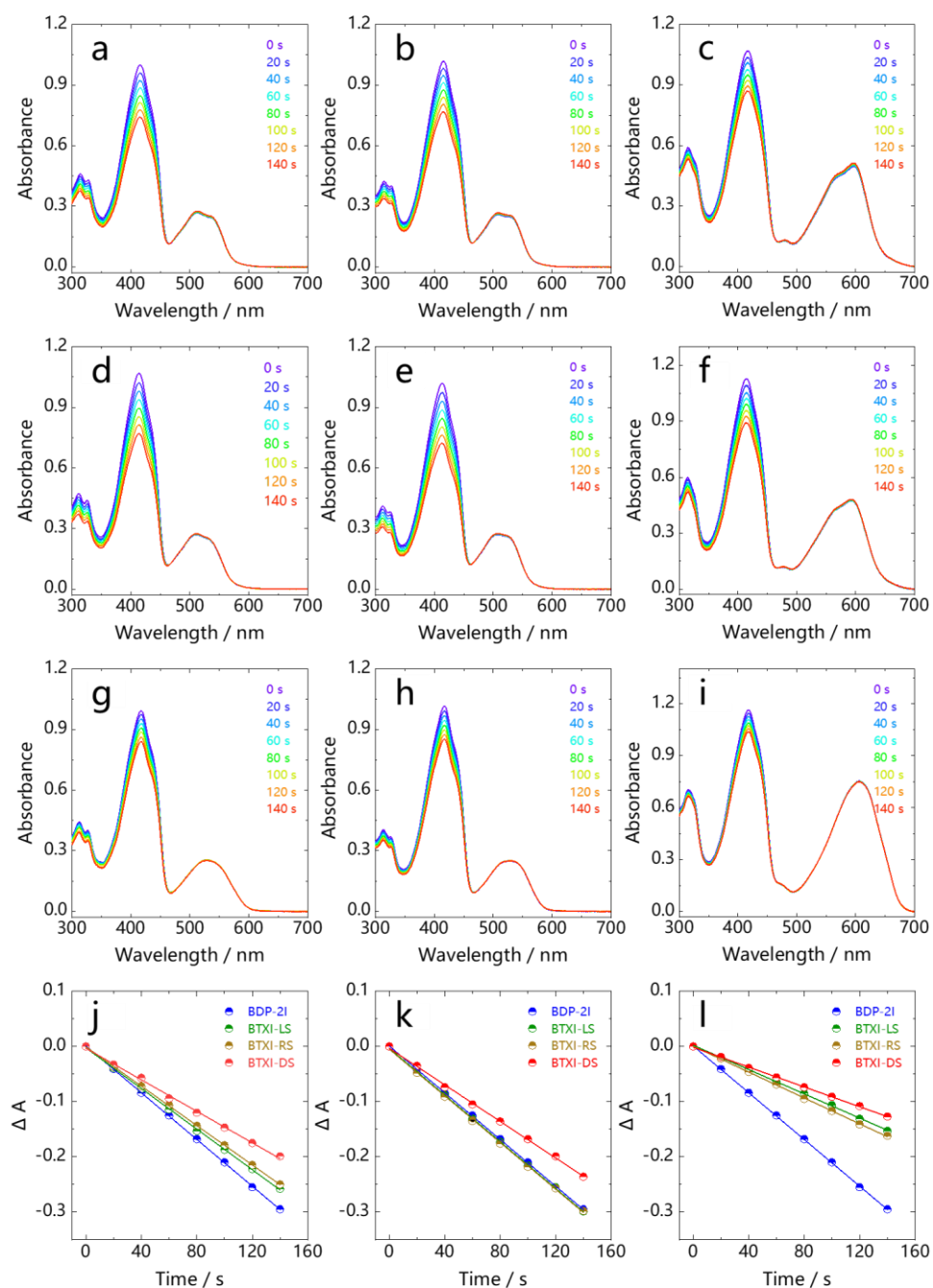
6. Singlet Oxygen Quantum Yield

Figure S16. Changes in the absorption of DPBF within time upon photo irradiating with 530 nm light in air saturated solution of DPBF and photosensitizer. Condition: **BTXI-LS** (a), **BTXI-RS** (b), **BTXI-DS** (c) in toluene; **BTXI-LS** (d), **BTXI-RS** (e), **BTXI-DS** (f) in 1,4-Dioxane and **BTXI-LS** (g), **BTXI-RS** (h), **BTXI-DS** (i) in DMSO. Kinetics of the singlet oxygen ($^1O_2$) photosensitization of the **BTXI-LS**, **BTXI-RS**, **BTXI-DS** respectively in toluene (j), 1,4-Dioxane (k), DMSO (l).
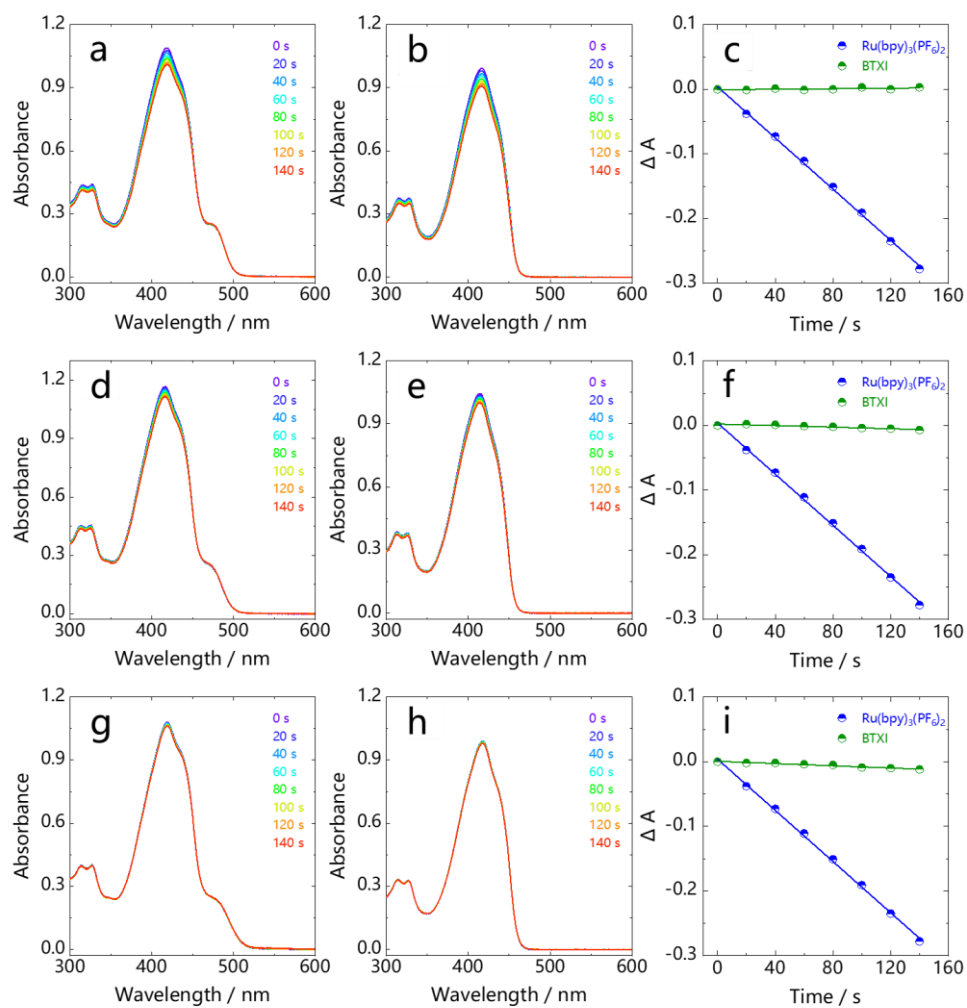
Figure S17. Changes in the absorption of DPBF within time upon photo irradiating with 460 nm light in air saturated solution of DPBF and photosensitizer. Condition: **BTXI** (a), DPBF (b) in toluene; **BTXI** (d), DPBF (e) in 1,4-Dioxane; **BTXI** (g), DPBF (h) in DMSO. Kinetics of the singlet oxygen ($^1O_2$) photosensitization of the **BTXI** respectively in toluene (c), 1,4-Dioxane (f), DMSO (i) and standard Ru(bpy)$_3$(PF$_6$)$_2$ in DCM.
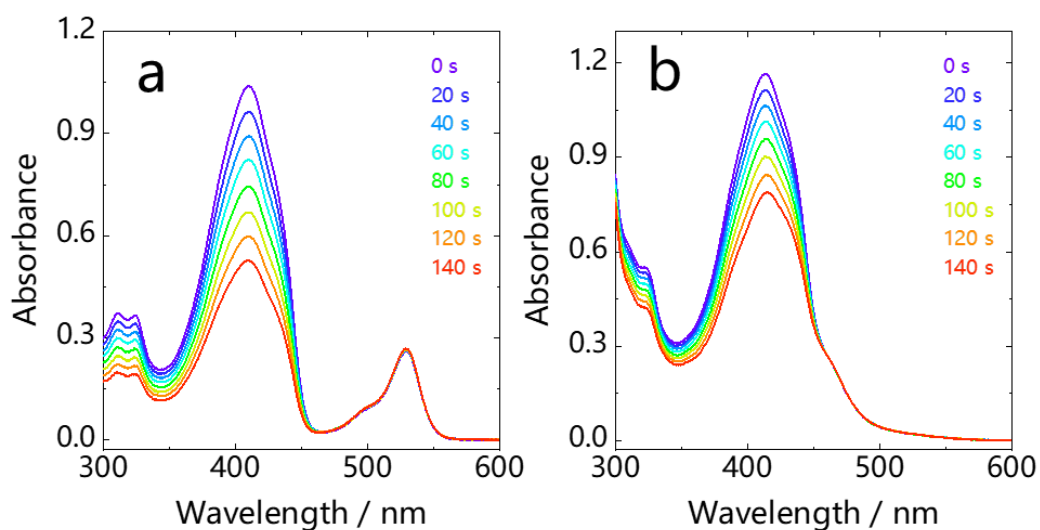
Figure S18. Changes in the absorption of DPBF within time upon photo irradiating in air saturated solution of DPBF and photosensitizer. Condition: BDP-2I (a) irradiated with 530 nm light in ACN, Ru(bpy)$_3$(PF$_6$)$_2$ (b) irradiated with 460 nm light in DCM.

Table S1: Photophysical parameters of compounds in 1,4-Dioxane.

Compounds	λ_{abs}[a]	ε[b]	λ_{em}[c]	Φ_F[d]	τ_F[e]	τ_T[f]	Φ_Δ[g]	Φ_{UC}[h]
BTXI	450	19200	505	99	7.39	–[i]	<1[j], <1, <1[k]	...
BTXI-LS	510	18400	–[i]	<0.1	–[i]	6.2[j], 8.5, 11.5[k]	95[j], 97, 54[k]	9.2[j], 13.6, 1.7[k]
BTXI-RS	506	21000	–[i]	<0.1	–[i]	11.7[j], 17.7, 23.5[k]	92[j], 97, 58[k]	10.1[j], 13.8, 1.2[k]
BTXI-DS	597	20900	–[i]	<0.1	–[i]	4.6[j], 5.1, 8.0[k]	72[j], 76, 44[k]	0.18[j], 1.3[j]

[a] Wavelength of strongest absorption, in nm; [b] Molar extinction coefficient, in M^{-1} cm^{-1}; [c] Wavelength of strongest emission, in nm; [d] Absolute fluorescence quantum yield, in nm; λ_{ex} = 420 nm; [e] Fluorescence lifetime, in ns; $c \approx 1.0 \times 10^{-5}$ M, λ_{ex} = 374 nm. [f] Triplet state lifetime, in μs; $c \approx 1.0 \times 10^{-5}$ M. [g] Singlet oxygen quantum yield, in %; BDP-2I as reference (Φ_Δ = 87%, in ACN). [h] Upconversion quantum yield, in %; [i] Not observed; [j] In toluene; [k] In DMSO.
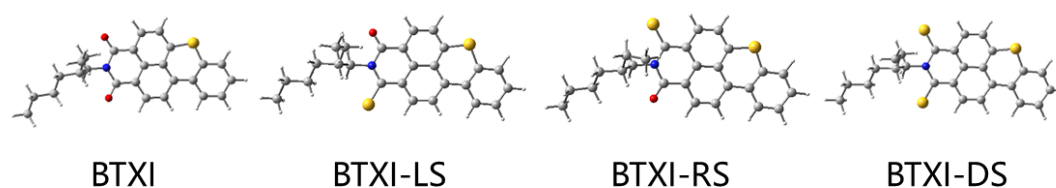
7. Density Functional Theory Calculations

Figure S19. Optimized ground state geometries of the compounds, calculated at the DFT (PBE0/6-31G(d,p)) level with Gaussian 16W.
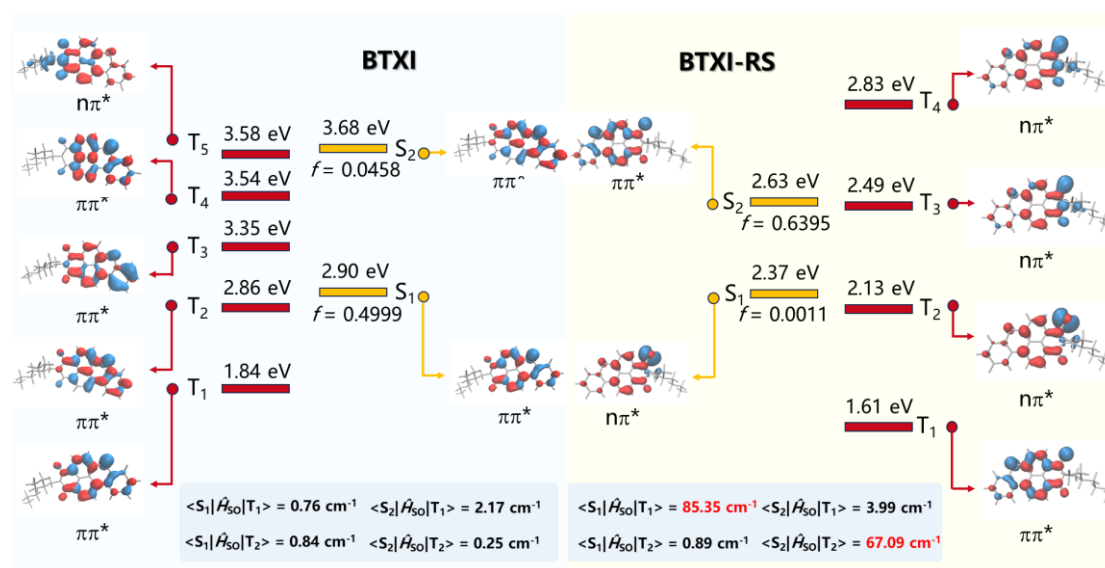

Figure S20. Selected frontier molecular orbitals involved in the excitation and triplet excited states of **BTXI** and **BTXI-RS**. Spin-orbit coupling matrix elements between S_n and T_n states of **BTXI** and **BTXI-RS**.
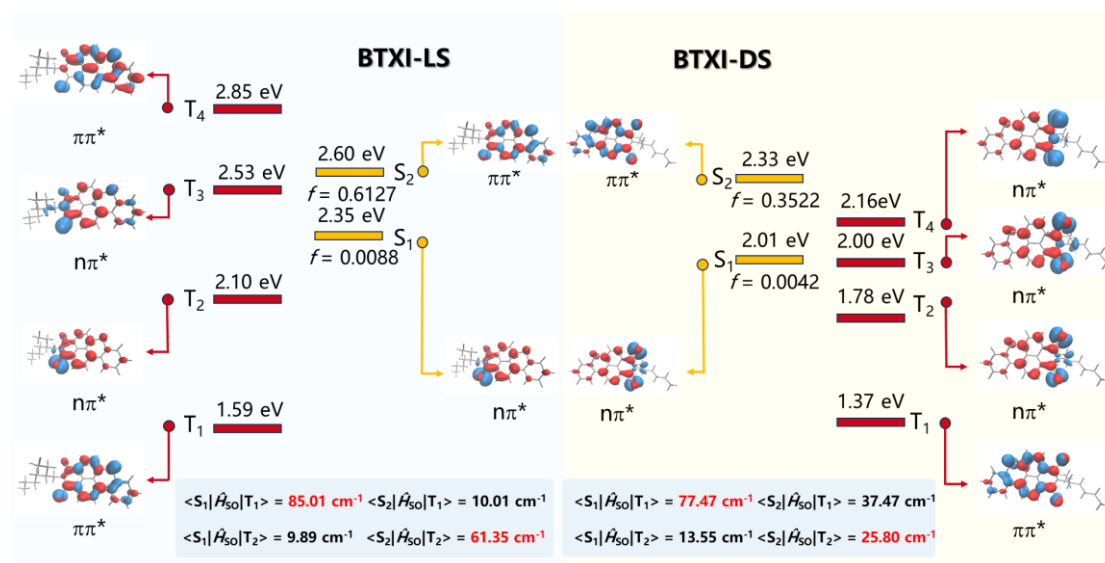
Figure S21. Selected frontier molecular orbitals involved in the excitation and triplet excited states of **BTXI-LS** and **BTXI-DS**. Spin-orbit coupling matrix elements between S_n and T_n states of **BTXI-LS** and **BTXI-DS**.

Table S2: Selected parameters of the excited states of **BTXI-LS**. Excited states of the **BTXI-LS** calculated by DFT//PBE0/6-31G (d,p) based on the optimized ground state geometry.

BTXI-LS	Electronic transition	DFT//PBE0/6-31G (d,p)		
		Excitation energy	f [a]	$\Delta E_{S_1-T_1}$
Absorption	$S_0 \rightarrow S_1$	2.35^b, 2.34^c, 2.47^d	0.0106^b, 0.0088^c, 0.0636^d	0.764^b
	$S_0 \rightarrow S_2$	2.58^b, 2.59^c, 2.56^d	0.6276^b, 0.6127^c, 0.5624^d	$0.759^{c,}$
Triplet States	$S_0 \rightarrow T_1$	1.59^b, 1.58^c, 1.61^d	0.0000^b, 0.000^c, 0.0000^d	0.863^d
	$S_0 \rightarrow T_2$	2.10^b, 2.10^c, 2.24^d	0.0000^b, 0.000^c, 0.0000^d	

[a] Oscillator strength; [b] In Toluene; [c] In 1,4-Dioxane; [d] In DMSO.

Table S3: Selected parameters of the excited states of **BTXI-RS**. Excited states of the **BTXI-RS** calculated by DFT//PBE0/6-31G (d,p) based on the optimized ground state geometry.

BTXI-RS	Electronic transition	DFT//PBE0/6-31G (d,p)		
		Excitation energy	f [a]	$\Delta E_{S_1-T_1}$
Absorption	$S_0 \rightarrow S_1$	2.38^b, 2.37^c, 2.50^d	0.0013^b, 0.0011^c, 0.0074^d	0.772^b
	$S_0 \rightarrow S_2$	2.61^b, 2.62^c, 2.60^d	0.6578^b, 0.6395^c, 0.6621^d	0.767^c
Triplet States	$S_0 \rightarrow T_1$	1.61^b, 1.60^c, 1.63^d	0.0000^b, 0.000^c, 0.0000^d	0.871^d
	$S_0 \rightarrow T_2$	2.13^b, 2.13^c, 2.26^d	0.0000^b, 0.000^c, 0.0000^d	

[a] Oscillator strength; [b] In Toluene; [c] In 1,4-Dioxane; [d] In DMSO.

Table S4: Selected parameters of the excited states of **BTXI-DS**. Excited states of the **BTXI-DS** calculated by DFT//PBE0/6-31G (d,p) based on the optimized ground state geometry.

BTXI-DS	Electronic transition	DFT//PBE0/6-31G (d,p)		
		Excitation energy	f^a	$\Delta E_{S_1-T_1}$
Absorption	$S_0 \rightarrow S_1$	2.01^b, 2.01^c, 2.11^d	0.0048^b, 0.0042^c, 0.0114^d	0.642^b
	$S_0 \rightarrow S_2$	2.33^b, 2.33^c, 2.32^d	0.4769^b, 0.3522^c, 0.6488^d	0.638^c
Triplet States	$S_0 \rightarrow T_1$	1.37^b, 1.37^c, 1.38^d	0.0000^b, 0.000^c, 0.0000^d	0.728^d
	$S_0 \rightarrow T_2$	1.78^b, 1.78^c, 1.89^d	0.0000^b, 0.000^c, 0.0000^d	

[a] Oscillator strength; [b] In Toluene; [c] In 1,4-Dioxane; [d] In DMSO.

8. Nanosecond Transient Absorption Spectra
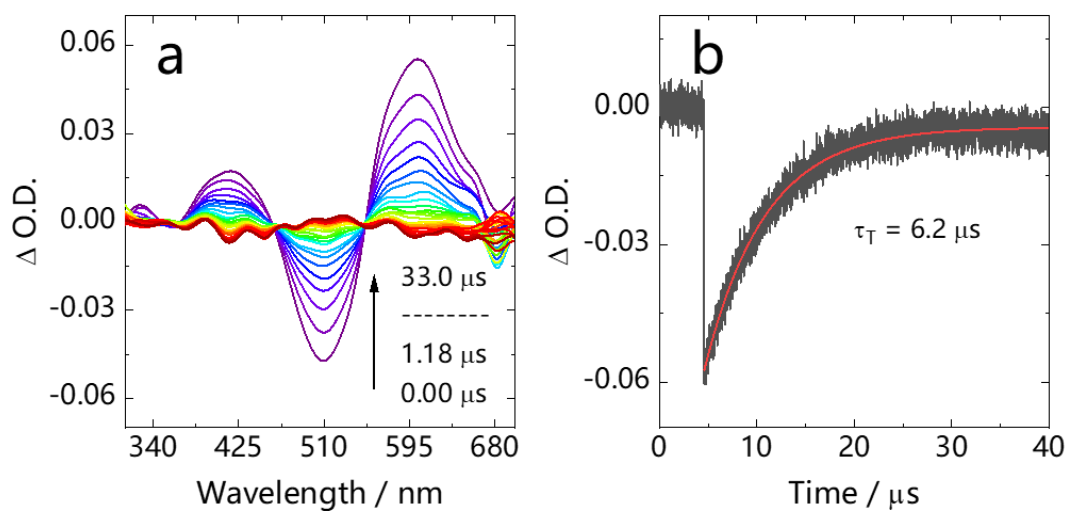
Figure S22. (a) Nanosecond transient absorption spectra of **BTXI-LS** at different decay time, λ_{ex} = 530 nm, $c \approx 1 \times 10^{-5}$ M, in toluene. (b) The decay curve of **BTXI-LS** at 510 nm, $c \approx 1 \times 10^{-5}$ M, in toluene.
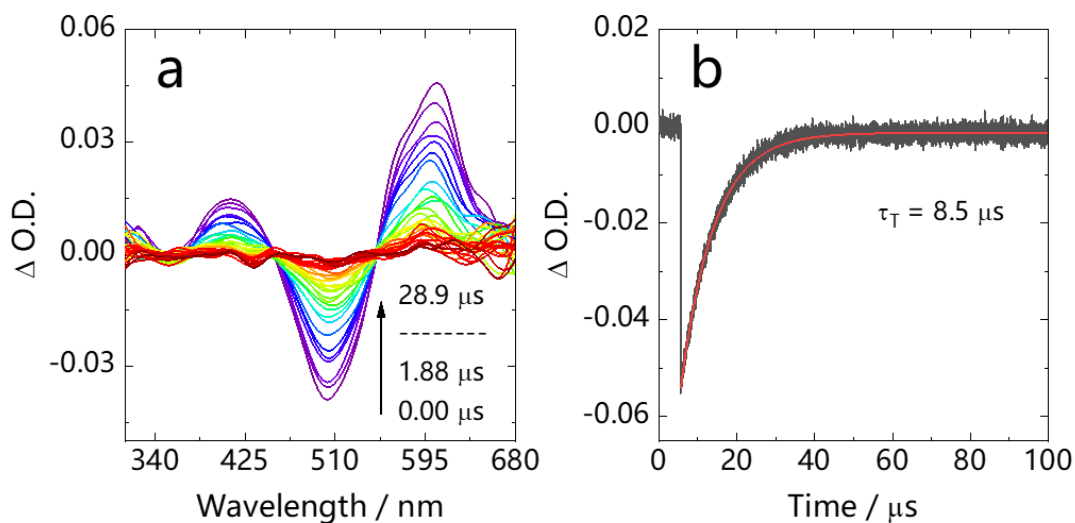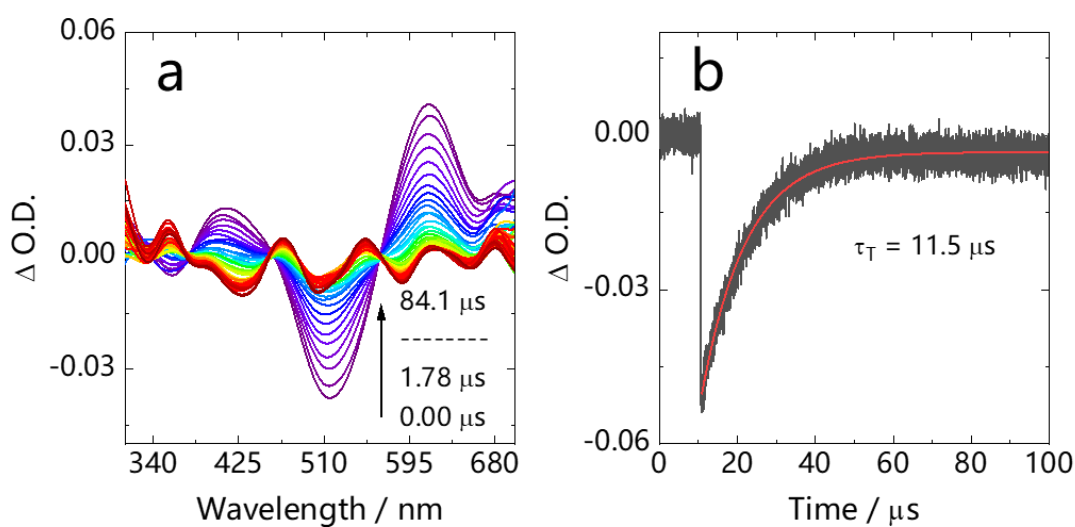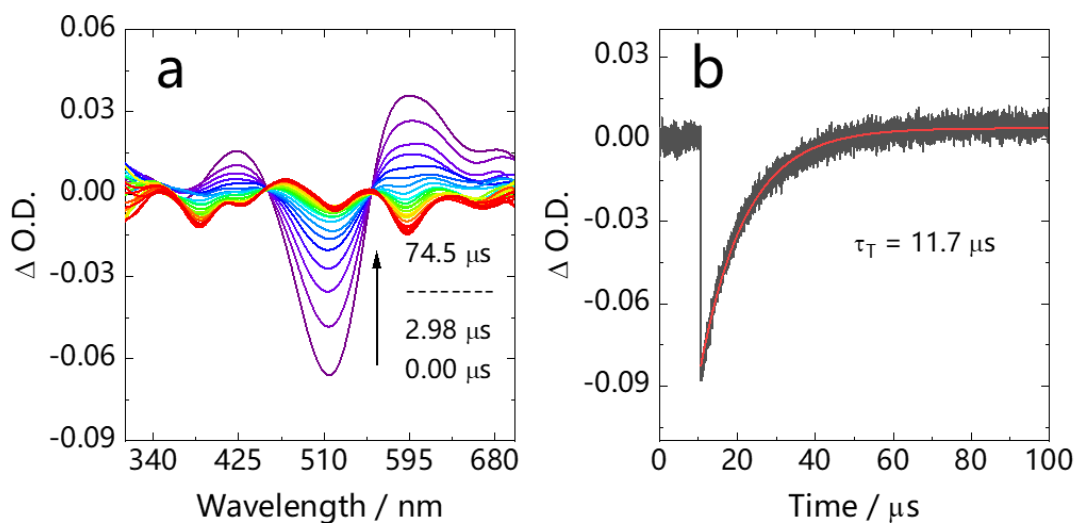
Figure S23. (a) Nanosecond transient absorption spectra of **BTXI-LS** at different decay time, λ_{ex} = 530 nm, c ≈ 1 × 10^{-5} M, in 1,4-Dioxane. (b) The decay curve of **BTXI-LS** at 510 nm, c ≈ 1 × 10^{-5} M, in 1,4-Dioxane.

Figure S24. (a) Nanosecond transient absorption spectra of **BTXI-LS** at different decay time, λ_{ex} = 530 nm, c ≈ 1 × 10^{-5} M, in DMSO. (b) The decay curve of **BTXI-LS** at 510 nm, c ≈ 1 × 10^{-5} M, in DMSO.
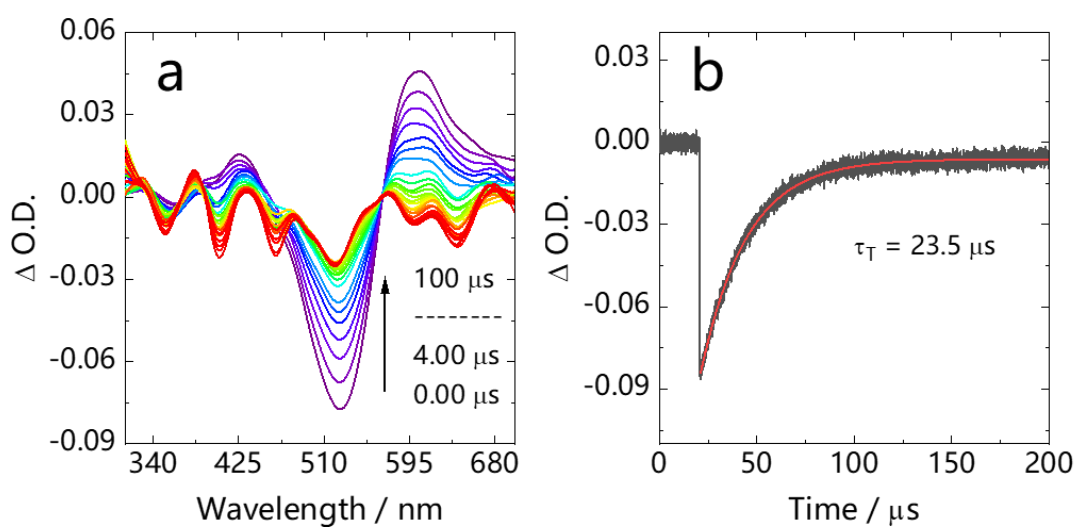
Figure S25. (a) Nanosecond transient absorption spectra of **BTXI-RS** at different decay time, λ_{ex} = 530 nm, $c \approx 1 \times 10^{-5}$ M, in toluene. (b) The decay curve of **BTXI-RS** at 510 nm, $c \approx 1 \times 10^{-5}$ M, in toluene.

Figure S26. (a) Nanosecond transient absorption spectra of **BTXI-RS** at different decay time, λ_{ex} = 530 nm, $c \approx 1 \times 10^{-5}$ M, in DMSO. (b) The decay curve of **BTXI-RS** at 510 nm, $c \approx 1 \times 10^{-5}$ M, in DMSO.

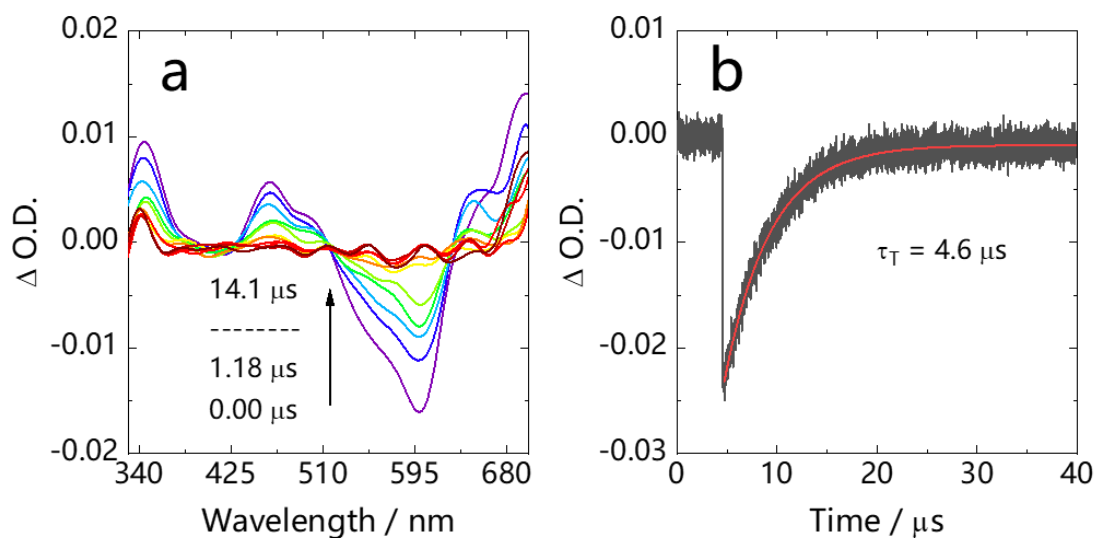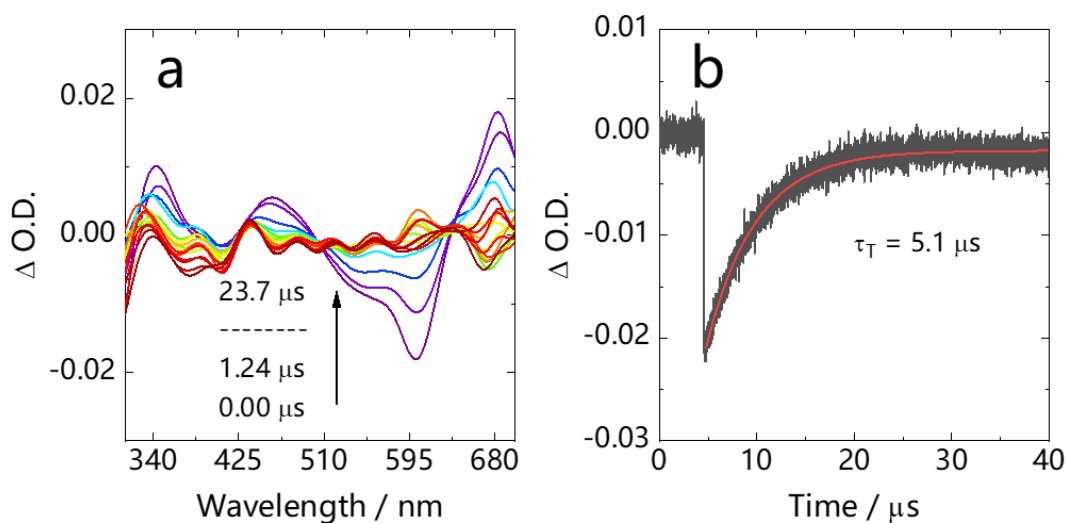**Figure S27.** (a) Nanosecond transient absorption spectra of **BTXI-DS** at different decay time, λ_{ex} = 610 nm, $c \approx 1 \times 10^{-5}$ M, in toluene. (b) The decay curve of **BTXI-DS** at 600 nm, $c \approx 1 \times 10^{-5}$ M, in toluene.

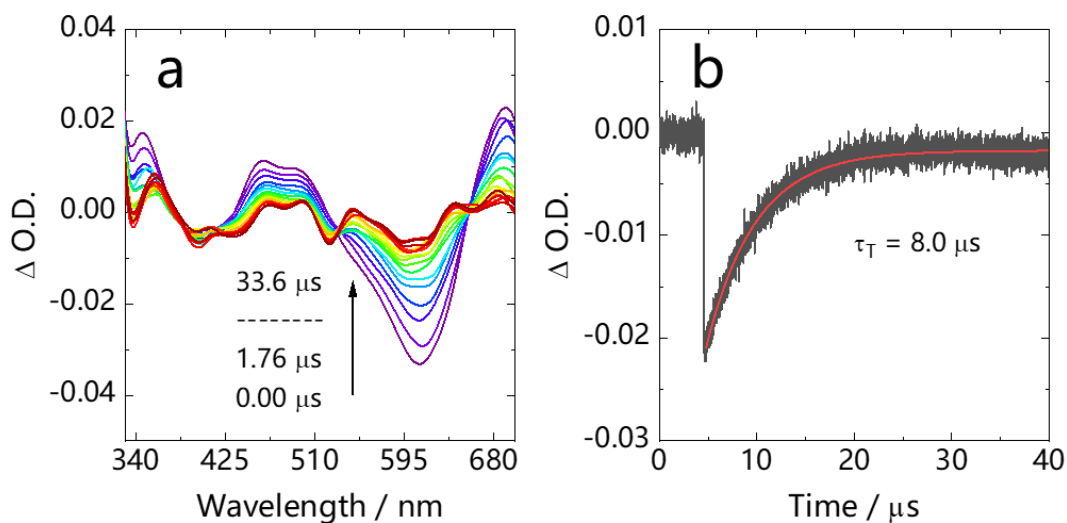**Figure S28.** (a) Nanosecond transient absorption spectra of **BTXI-DS** at different decay time, λ_{ex} = 610 nm, $c \approx 1 \times 10^{-5}$ M, in 1,4-Dioxane. (b) The decay curve of **BTXI-DS** at 600 nm, $c \approx 1 \times 10^{-5}$ M, in 1,4-Dioxane.

Figure S29. (a) Nanosecond transient absorption spectra of **BTXI-DS** at different decay time, λ_{ex} = 610 nm, $c \approx 1 \times 10^{-5}$ M, in DMSO. (b) The decay curve of **BTXI-DS** at 600 nm, $c \approx 1 \times 10^{-5}$ M, in DMSO.

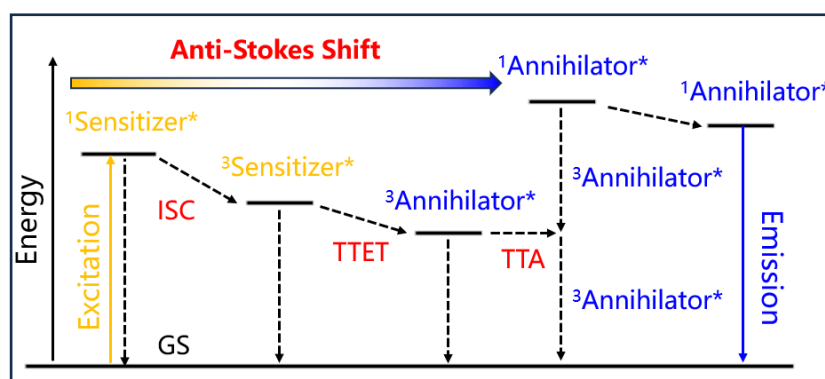## 9. Triplet-Triplet Annihilation Upconversion

Figure S30. Schematic illustration of the TTA-UC system, where GS stands for ground state, ISC stands for intersystem crossing, TTET and TTA stand for triplet-triplet energy transfer and triplet-triplet annihilation, respectively.
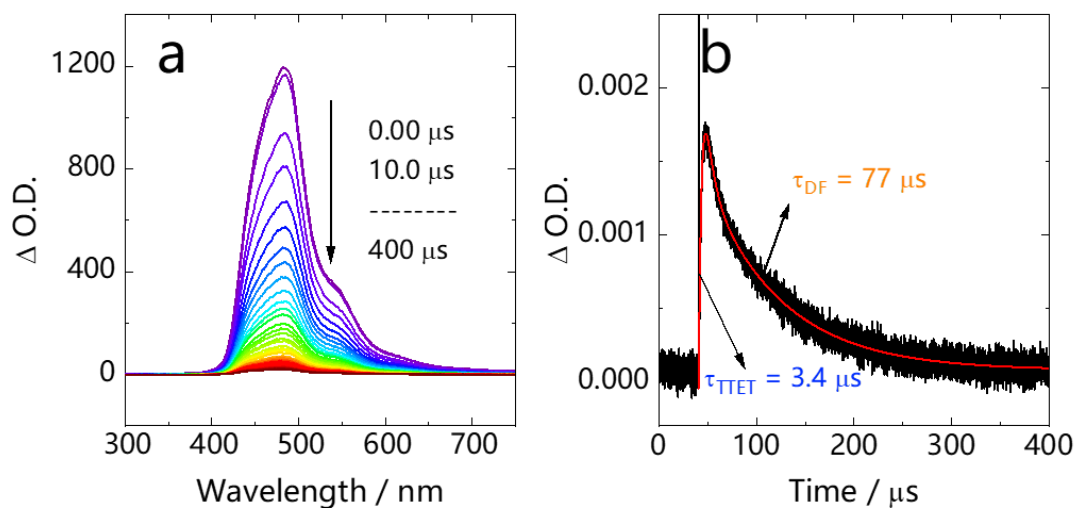
Figure S31. (a) Nanosecond transient emission spectra of **BTXI-LS** in the presence of Perylene (1×10^{-4} M), in 1,4-Dioxane. (b) The decay kinetic traces of compound at 470 nm. λ_{ex} = 530 nm.
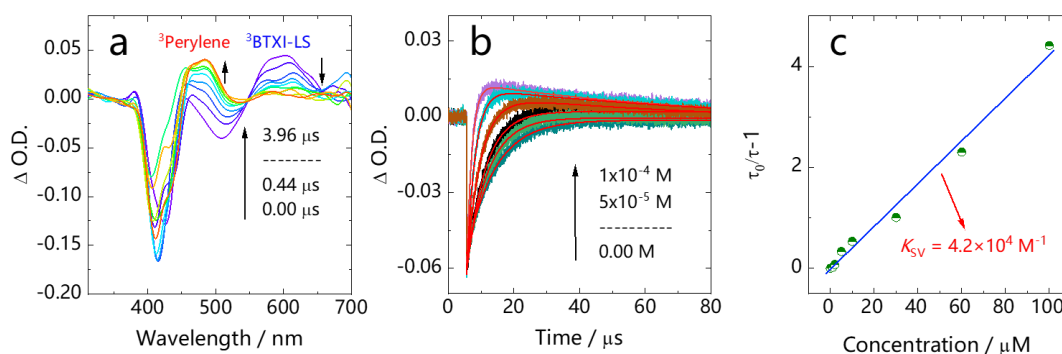

Figure S32. (a) Nanosecond transient absorption spectra of the mixed **BTXI-LS** (1×10^{-5} M) with Perylene (1×10^{-4} M) solution at different decay time. (b) Decay traces of the **BTXI-LS** (1×10^{-5} M) at 510 nm in the presence of different Perylene concentrations, in deaerated 1,4-Dioxane, λ_{ex} = 530 nm. (c) Stern-Volmer plot for lifetime quenching of **BTXI-LS** with increasing concentration of Perylene.
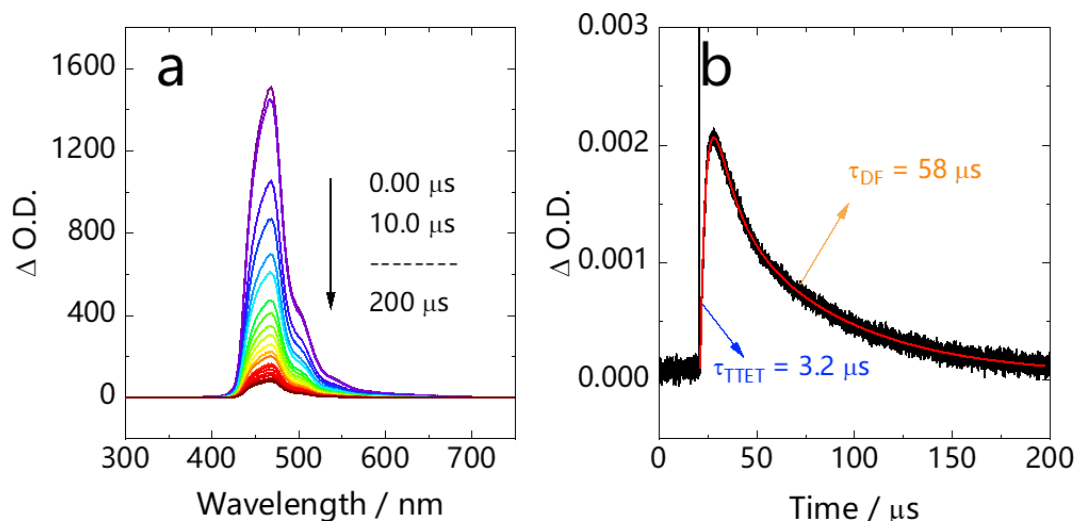
Figure S33. (a) Nanosecond transient emission spectra of **BTXI-RS** in the presence of Perylene (1×10^{-4} M), in 1,4-Dioxane. (b) The decay kinetic traces of compound at 470 nm. λ_{ex} = 530 nm.
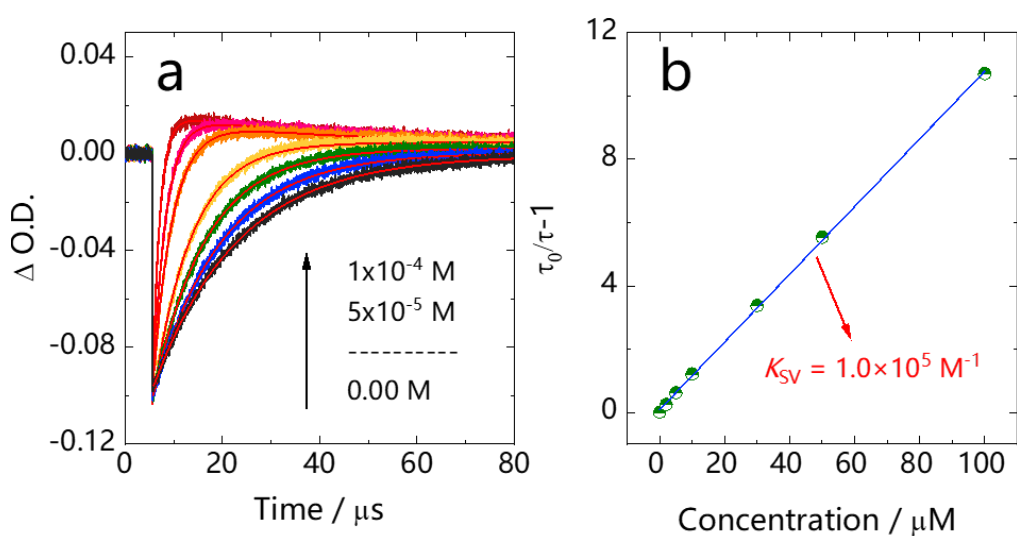

Figure S34. (a) Decay traces of the **BTXI-RS** (1×10^{-5} M) at 510 nm in the presence of different Perylene concentrations, in deaerated 1,4-Dioxane, λ_{ex} = 530 nm. (b) Stern-Volmer plot for lifetime quenching of **BTXI-RS** with increasing concentration of Perylene.
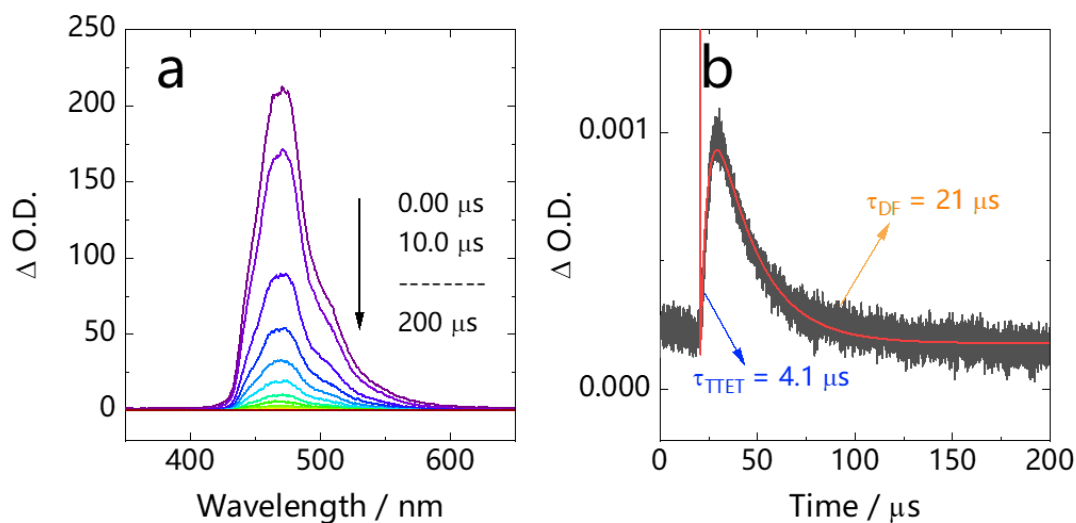
Figure S35. (a) Nanosecond transient emission spectra of **BTXI-DS** in the presence of TIPS-AC (1×10^{-4} M), in toluene. (b) The decay kinetic traces of compound at 470 nm. λ_{ex} = 610 nm.

Figure S36. (a) Nanosecond transient absorption spectra of the mixed **BTXI-DS** (1×10^{-5} M) with TIPS-AC (1×10^{-4} M) solution at different decay time. (b) Decay traces of the **BTXI-DS** (1×10^{-5} M) at 600 nm in the presence of different TIPS-AC concentrations, in deaerated toluene, λ_{ex} = 610 nm. (c) Stern-Volmer plot for lifetime quenching of **BTXI-DS** with increasing concentration of TIPS-AC.
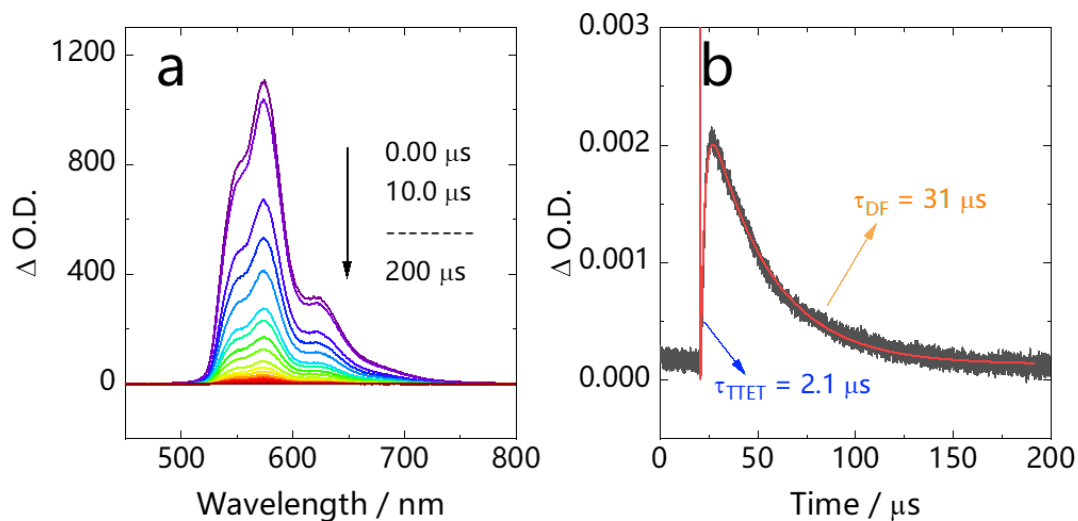
Figure S37. (a) Nanosecond transient emission spectra of **BTXI-DS** in the presence of PBI (1×10^{-4} M), in toluene. (b) The decay kinetic traces of compound at 540 nm. λ_{ex} = 610 nm.
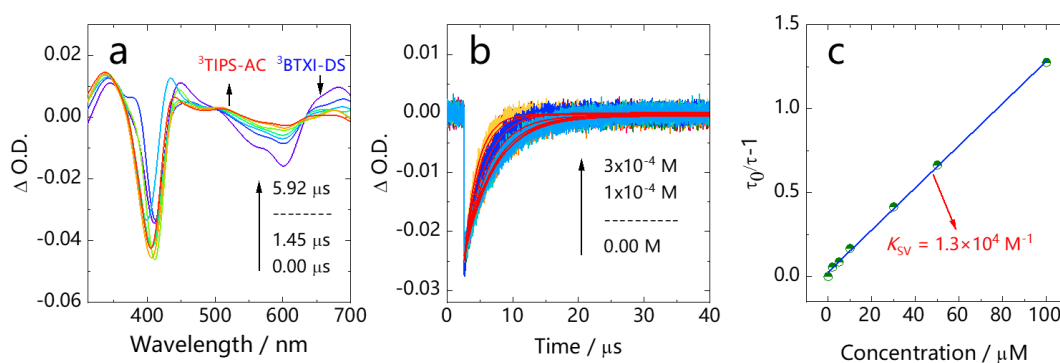

Figure S38. (a) Nanosecond transient absorption spectra of the mixed **BTXI-DS** (1×10^{-5} M) with PBI (1×10^{-4} M) solution at different decay time. (b) Decay traces of the **BTXI-DS** (1×10^{-5} M) at 600 nm in the presence of different PBI concentrations, in deaerated toluene, λ_{ex} = 610 nm. (c) Stern-Volmer plot for lifetime quenching of **BTXI-DS** with increasing concentration of PBI.
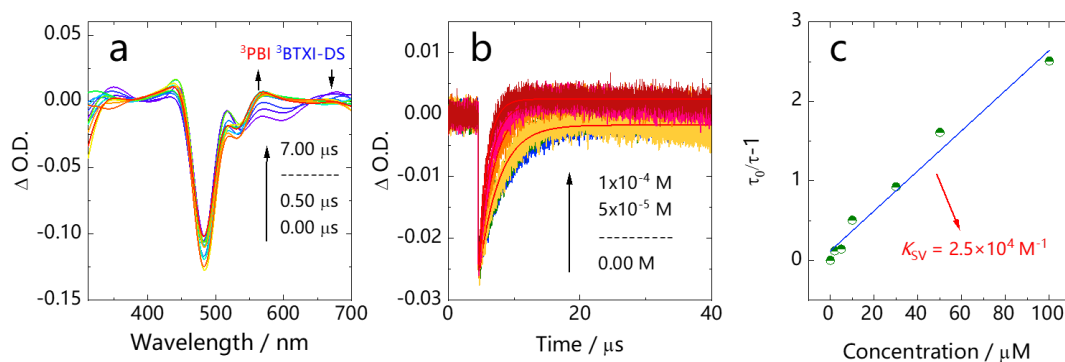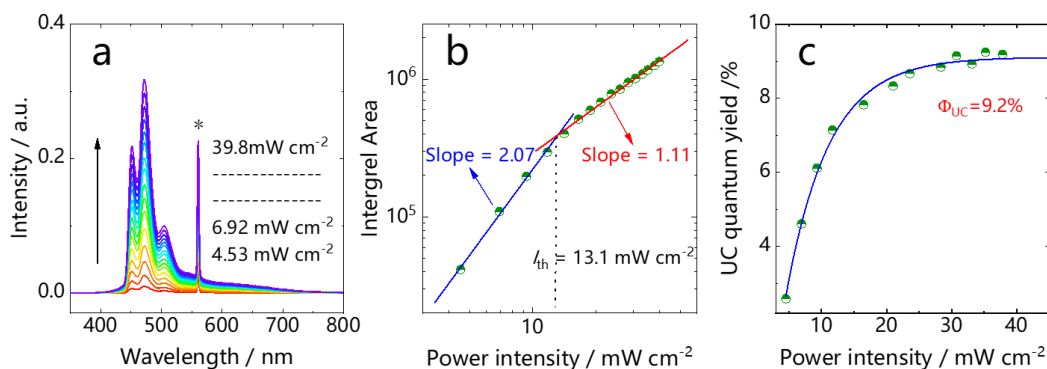
Figure S39. (a) TTA-UC spectra with **BTXI-LS** as the photosensitizer (1×10^{-5} M) and perylene as the acceptor (1×10^{-4} M) at different power density, λ_{ex} = 561 nm, in toluene. (b) Integrated upconversion fluorescence emission intensity of perylene plotted as a function of incident power density. (c) Upconversion quantum yield of perylene plotted as a function of incident power density.

Figure S40. (a) TTA-UC spectra with **BTXI-LS** as the photosensitizer (1×10^{-5} M) and perylene as the acceptor (1×10^{-4} M) at different power density, λ_{ex} = 561 nm, in 1,4-Dioxane. (b) Integrated upconversion fluorescence emission intensity of perylene plotted as a function of incident power density. (c) Upconversion quantum yield of perylene plotted as a function of incident power density.
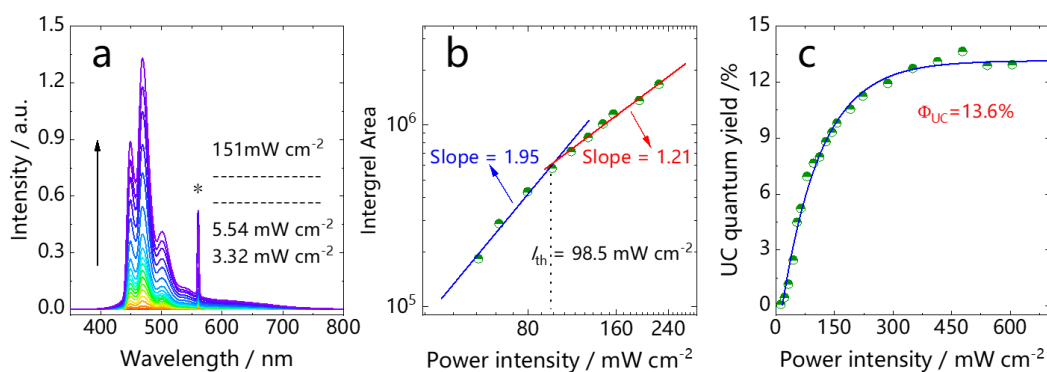
Figure S41. (a) TTA-UC spectra with **BTXI-LS** as the photosensitizer (1×10^{-5} M) and perylene as the acceptor (1×10^{-4} M) at different power density, λ_{ex} = 561 nm, in DMSO. (b) Integrated upconversion fluorescence emission intensity of perylene plotted as a function of incident power density. (c) Upconversion quantum yield of perylene plotted as a function of incident power density.
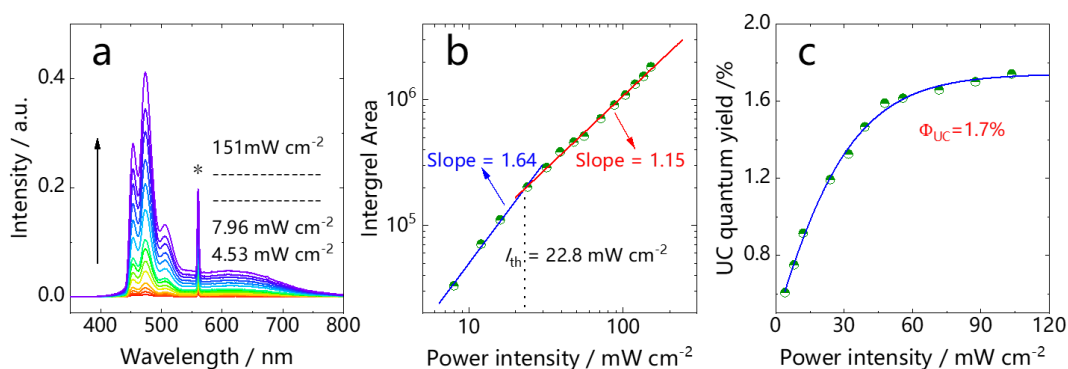

Figure S42. (a) TTA-UC spectra with **BTXI-RS** as the photosensitizer (1×10^{-5} M) and perylene as the acceptor (1×10^{-4} M) at different power density, λ_{ex} = 561 nm, in toluene. (b) Integrated upconversion fluorescence emission intensity of perylene plotted as a function of incident power density. (c) Upconversion quantum yield of perylene plotted as a function of incident power density.
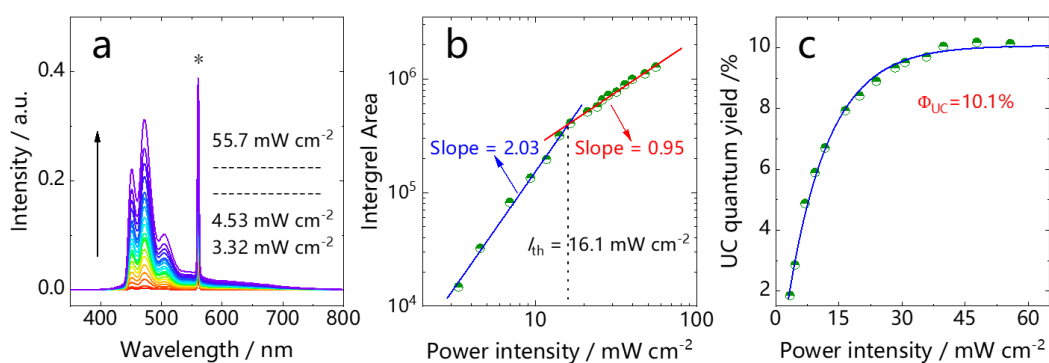
Figure S43. (a) TTA-UC spectra with **BTXI-RS** as the photosensitizer (1×10^{-5} M) and perylene as the acceptor (1×10^{-4} M) at different power density, λ_{ex} = 561 nm, in DMSO. (b) Integrated upconversion fluorescence emission intensity of perylene plotted as a function of incident power density. (c) Upconversion quantum yield of perylene plotted as a function of incident power density.
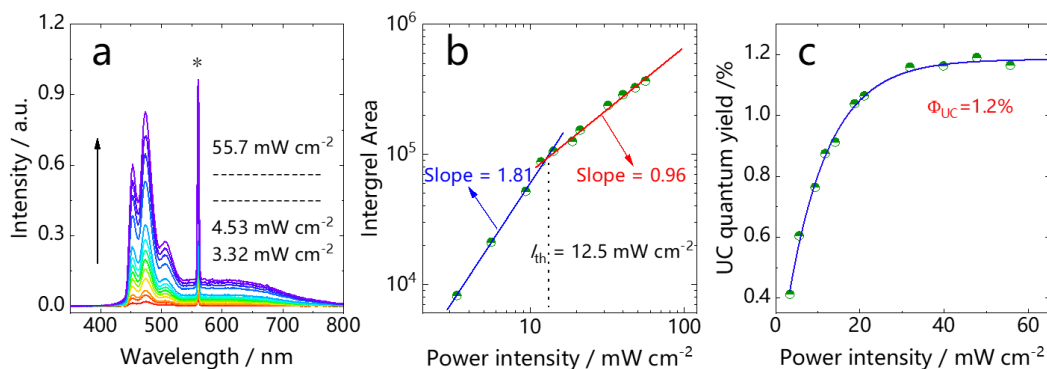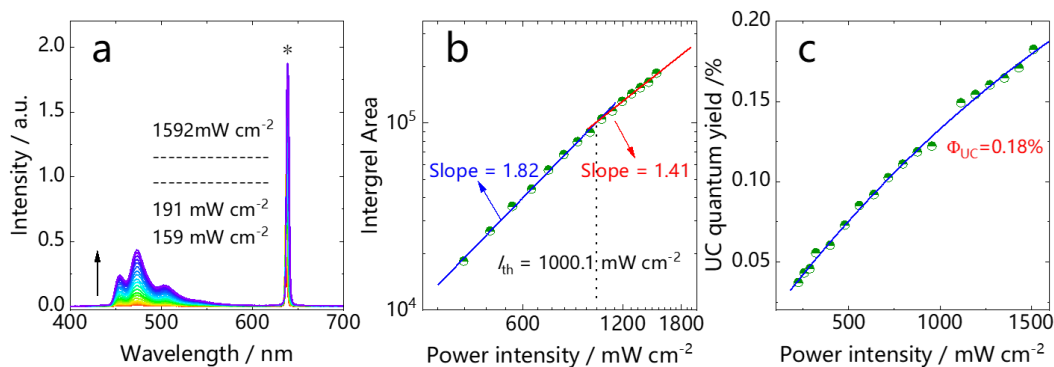

Figure S44. (a) TTA-UC spectra with **BTXI-DS** as the photosensitizer (1×10^{-5} M) and TIPS-AC as the acceptor (1×10^{-4} M) at different power density, λ_{ex} = 635 nm, in toluene. (b) Integrated upconversion fluorescence emission intensity of TIPS-AC plotted as a function of incident power density. (c) Upconversion quantum yield of TIPS-AC plotted as a function of incident power density.

Figure S45. (a) TTA-UC spectra with **BTXI-DS** as the photosensitizer (1×10^{-5} M) and PBI as the acceptor (1×10^{-4} M) at different power density, λ_{ex} = 635 nm, in toluene. (b) Integrated upconversion fluorescence emission intensity of PBI plotted as a function of incident power density. (c) Upconversion quantum yield of PBI plotted as a function of incident power density.
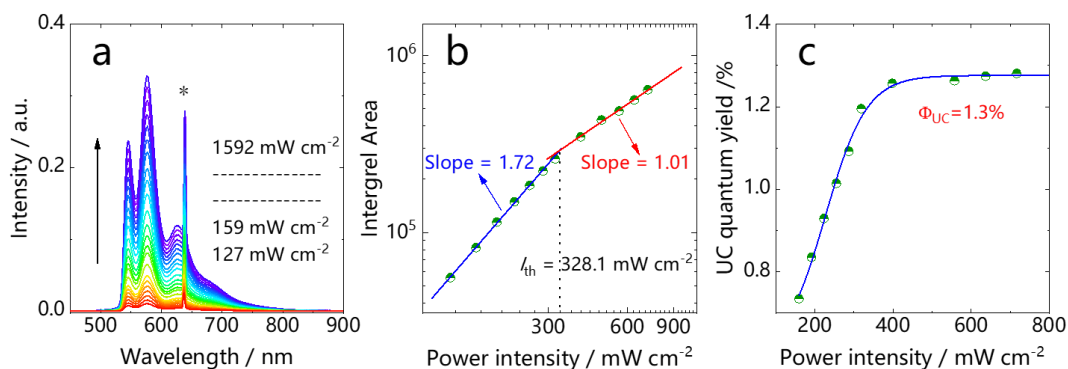
10. Photopolymerization

Figure S46. The experiment for the polymerization of monomer (DMA), conditions: **BTXI-DS**, diphenyliodonium salt, irradiated for 5 minutes with the wavelength of LED is 630 nm (100 mW cm^{-2}).

Figure S47. The experiment for the polymerization of monomer (EEEA), conditions: **BTXI-DS**, diphenyliodonium salt, irradiated for 5 minutes with the wavelength of LED is 630 nm (100 mW cm^{-2}).

Figure S48. The experiment for the polymerization of monomer (IBOA), conditions: **BTXI-DS**, diphenyliodonium salt, irradiated for 5 minutes with the wavelength of LED is 630 nm (100 mW cm^{-2}).
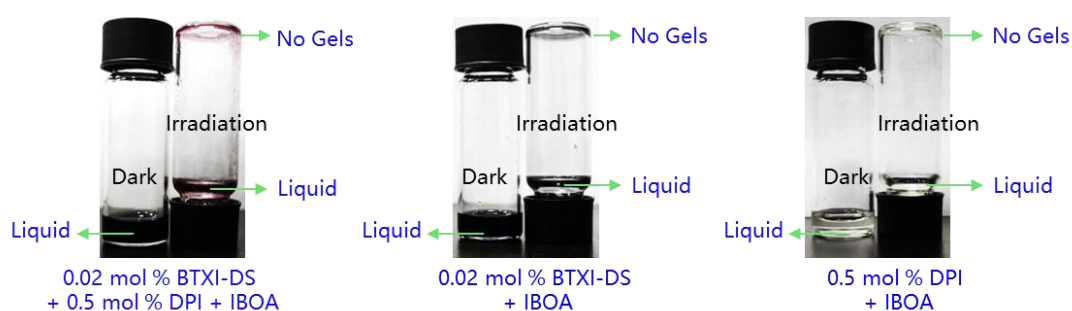

Figure S49. The experiment for the polymerization of monomer (DMA), conditions: **BTXI-RS**, diphenyliodonium salt, irradiated for 5 minutes with the wavelength of optical fiber is 532 nm (100 mW cm^{-2}).

Figure S50. The experiment for the polymerization of monomer (EEEA), conditions: **BTXI-RS**, diphenyliodonium salt, irradiated for 5 minutes with the wavelength of optical fiber is 532 nm (100 mW cm^{-2}).

Figure S51. The experiment for the polymerization of monomer (IBOA), conditions: **BTXI-RS**, diphenyliodonium salt, irradiated for 5 minutes with the wavelength of optical fiber is 532 nm (100 mW cm^{-2}).

Figure S52. The UV-Vis absorption spectra in different conditions. (a) **BTXI-DS** (5×10^{-5} M), diphenyliodonium salt (4×10^{-2} M). (b) **BTXI-DS** (5×10^{-5} M). The wavelength of LED is 630 nm (100 mW cm^{-2}). In ACN.
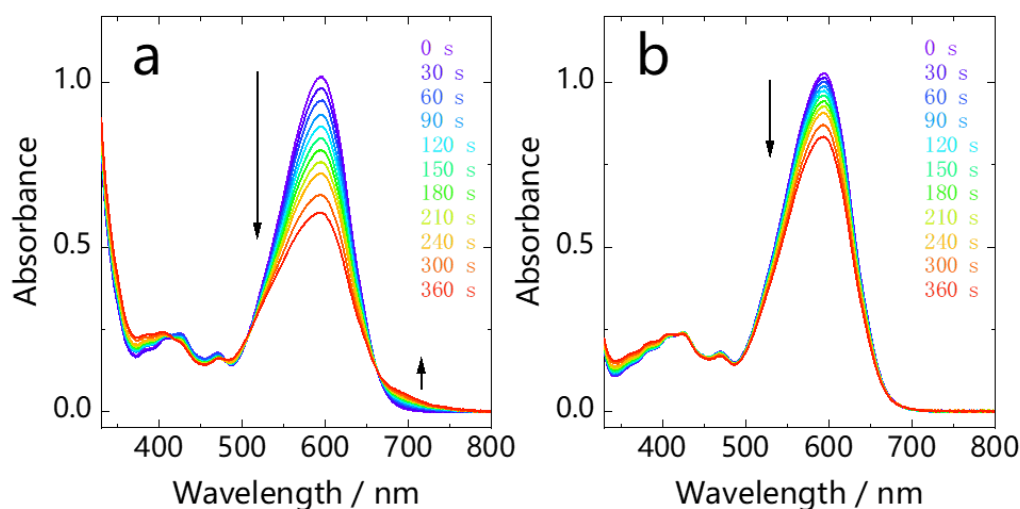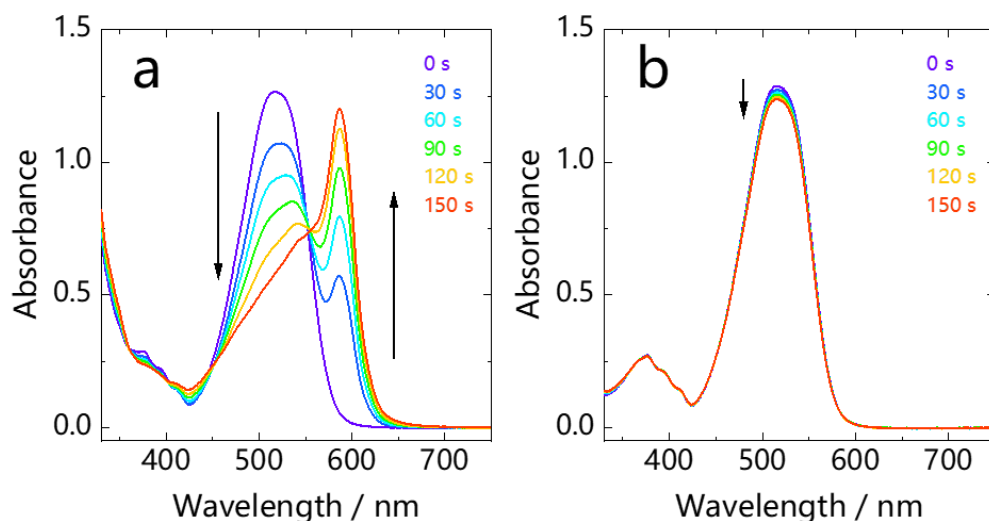
Figure S53. The UV-Vis absorption spectra in different conditions. (a) **BTXI-RS** (5×10^{-5} M), diphenyliodonium salt (4×10^{-2} M). (b) **BTXI-RS** (5×10^{-5} M). The wavelength of irradiation optical fiber is 532 nm (100 mW cm^{-2}). In ACN.
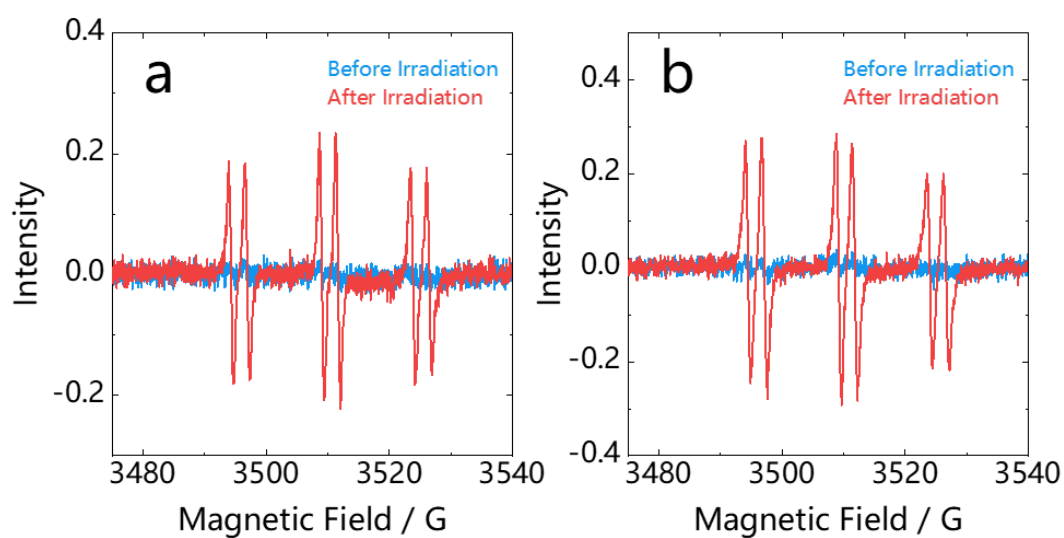

Figure S54. (a) The EPR spectra of **BTXI-DS** by using α-phenyl-N-tert-butylnitrone (PBN) as radical scavenge. Conditions: **BTXI-DS** (1×10^{-3} M), diphenyliodonium salt (1.5×10^{-3} M), PBN (1×10^{-2} M), in DMSO, irradiated for 5 minutes with the wavelength of LED is 630 nm (100 mW cm^{-2}). (b) The EPR spectra of **BTXI-RS** by using PBN as radical scavenge. Conditions: **BTXI-RS** (1×10^{-3} M), diphenyliodonium salt (1.5×10^{-3} M), PBN (1×10^{-2} M), in DMSO, irradiated for 5 minutes with the wavelength of optical fiber is 532 nm (100 mW cm^{-2}).

Table S5. The molecular weight and dispersity values of the polymers prepared by photopolymerization reactions after 5 minutes of irradiation (λ_{ex}= 532 nm, 100 mW cm^{-2}).

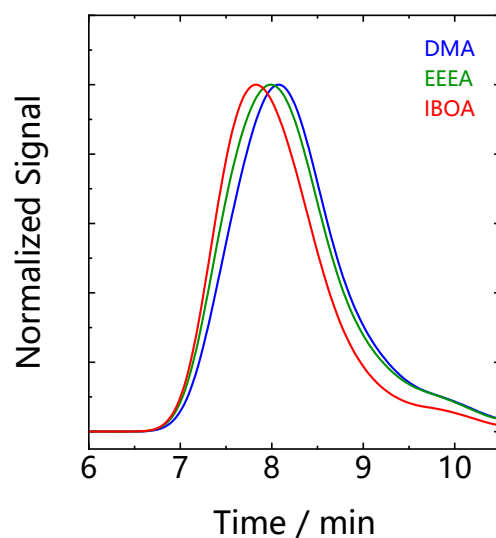| Monomer	M_n (Da)	M_w (Da)	PDI
DMA	12086	36518	3.02
EEEA	13799	42653	3.09
IBOA	16262	49139	3.02

Figure S55. The GPC chromatograms of the polymers prepared by photopolymerization reactions after 5 minutes of irradiation (λ_{ex}= 532 nm, 100 mW cm^{-2}). Conditions: **BTXI-RS** as the photoinitiator, **DPI** as the co-initiator, and **IBOA**, **EEEA**, and **DMA** as monomers.

Reference

1 H. Liang, M. Lu, Z. Mahmood, Z. Li, Z. Chen, G. Chen, M. Li, Y. Huo and S. Ji, *Angew. Chem. Int. Ed.*, 2023, **62**, e202312600.

2 Z. Chen, Z. Mahmood, H. Liang, Y. Wen, Y. Huo and S. Ji, *Dyes. Pigm.*, 2023, **219**, 111636.

3 Gaussian 16, Revision C.01, M. J. Frisch, G. W. Trucks, H. B. Schlegel, G. E. Scuseria, M. A. Robb, J. R. Cheeseman, G. Scalmani, V. Barone, G. A. Petersson, H. Nakatsuji, X. Li, M. Caricato, A. V. Marenich, J. Bloino, B. G. Janesko, R. Gomperts, B. Mennucci, H. P. Hratchian, J. V. Ortiz, A. F. Izmaylov, J. L. Sonnenberg, D. Williams-Young, F. Ding, F. Lipparini, F. Egidi, J. Goings, B. Peng, A. Petrone, T. Henderson, D. Ranasinghe, V. G. Zakrzewski, J. Gao, N. Rega, G. Zheng, W. Liang, M. Hada, M. Ehara, K. Toyota, R. Fukuda, J. Hasegawa, M. Ishida, T. Nakajima, Y. Honda, O. Kitao, H. Nakai, T. Vreven, K. Throssell, J. A. Montgomery, Jr., J. E. Peralta, F. Ogliaro, M. J. Bearpark, J. J. Heyd, E. N. Brothers, K. N. Kudin, V. N. Staroverov, T. A. Keith, R. Kobayashi, J. Normand, K. Raghavachari, A. P. Rendell, J. C. Burant, S. S. Iyengar, J. Tomasi, M. Cossi, J. M. Millam, M. Klene, C. Adamo, R. Cammi, J. W. Ochterski, R. L. Martin, K. Morokuma, O. Farkas, J. B. Foresman, and D. J. Fox, Gaussian, Inc., Wallingford CT, 2016.

4 A. M. Kadhim and A. T. Peters, *Tetrahedron*, 1974, **30**, 2245–2249.

5 P. Josse, S. Li, S. Dayneko, D. Joly, A. Labrunie, S. Dabos-Seignon, M. Allain, B. Siegler, R. Demadrille, G. C. Welch, C. Risko, P. Blanchard and C. Cabanetos, *J. Mater. Chem. C*, 2018, **6**, 761–766.

6 H. Liang, X. Zhang, M. Lu, X. Chen, W. Li, S. Li, M. Li, J. Zhao, Y. Huo and S. Ji, *Angew. Chem. Int. Ed.*, 2024, **63**, e202402774.